

MASTER

LBL-9429



Lawrence Berkeley Laboratory

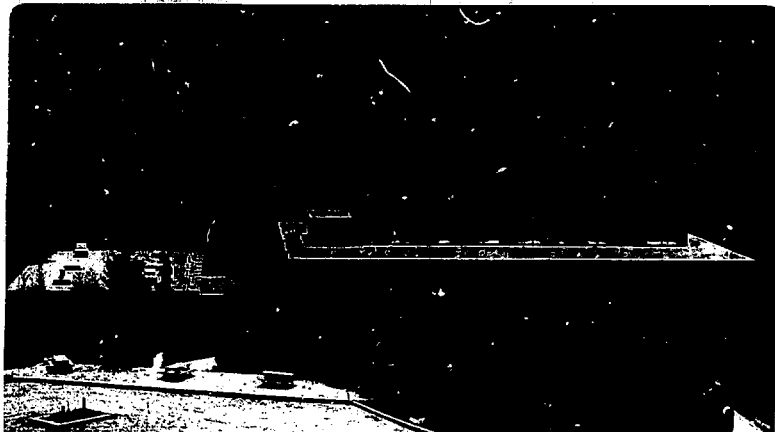
UNIVERSITY OF CALIFORNIA

**Materials & Molecular
Research Division**

THE DETERMINATION OF ELECTRONIC STATES IN CRYSTALLINE
SEMICONDUCTORS AND METALS BY ANGLE-RESOLVED PHOTOEMISSION

Kenneth Alan Mills
(Ph. D. thesis)

August 1979



Prepared for the U. S. Department of Energy
under Contract W-7405-ENG-48

DISTRIBUTION OF THIS DOCUMENT IS UNLIMITED

THE DETERMINATION OF ELECTRONIC STATES IN
CRYSTALLINE SEMICONDUCTORS AND METALS
BY ANGLE-RESOLVED PHOTOEMISSION

Contents

ABSTRACT	v
I. INTRODUCTION	1
A. The Direct Transition Model	4
B. Competing Mechanisms and the Breakdown of Direct Transitions	8
1. Surface state photoemission	9
2. Polarization effects	10
3. Band gap photoemission	12
4. Density of states photoemission	12
5. Thermal broadening	13
6. Momentum broadening	14
7. Refraction	15
References	16
PART I. SEMICONDUCTOR STUDIES	
II. FINAL-STATE BANDS IN GaAs	21
A. Experimental	22
B. Direct Transition Analysis	23
C. Onset of Density of States Features	27
References	30
Figure Captions	33
Figures	34



III. INTERFACE STATES IN GaAs/Ge	40
A. Experimental	41
B. Results for Low Coverage	41
C. Results for Higher Coverage	44
References	47
Figure Captions	48
Figures	49

PART II. CLEAN METAL STUDIES

IV. DISPERSION RELATIONS AND RELATED PHENOMENA FOR THE (111) FACE OF Au AND Pt	62
A. Experimental	63
B. Dispersion Relations	65
C. Polarization Effects	74
D. Thermal Behaviour	77
E. Final-State-Dependent Features	81
F. Summary	85
References	87
Tables	91
Figure Captions	95
Figures	98
V. EMPIRICAL BANDS AND FINAL-STATE EFFECTS FOR THE (110) and (100) FACES OF Ag	112
A. Experimental	113
B. Spectral Features and Dispersion Relations	114
1. Ag(100)	114
2. Ag(110)	119
C. Final-State Effects	123
D. Summary	129
References	130
Tables	132
Figure Captions	134
Figures	136
ACKNOWLEDGMENTS	144

THE DETERMINATION OF ELECTRONIC STATES IN
CRYSTALLINE SEMICONDUCTORS AND METALS
BY ANGLE-RESOLVED PHOTOEMISSION

Kenneth Alan Mills

Materials and Molecular Research Division,
Lawrence Berkeley Laboratory and
Department of Chemistry, University of California,
Berkeley, California 94720

ABSTRACT

An important part of the theoretical description of the solid state is the concept of band structure, which relies on the existence of dispersion relations connecting the electronic energy and wavevector in materials with translational symmetry. These relations in large measure determine the electronic behaviour of such materials. The elaboration of accurate band structures, therefore, is of considerable fundamental and practical importance. Angle-resolved photoemission (ARP) spectroscopy provides the only presently available method for the detailed experimental investigation of band structures, and this work is concerned with its application to both semiconducting and metallic single crystals. A brief review is given of the principle concepts and formalisms necessary for empirical band-mapping using ARP. Attention is focussed primarily on the actual electromagnetic excitation process; both direct and indirect transitions are discussed, as are final-state dependent effects, and the influence of parameters such as radiative polarization, temperature, sampling depth, and experimental geometry. Part I of the

thesis is concerned with the application of ARP to semiconducting materials. Variable-photon-energy spectra are used to map conduction bands for the Σ and Σ' directions in GaAs, and the results are compared with theory. The electronic structure of this face is also investigated for successive epitaxial depositions of Ge in sub-monolayer amounts. States apparently associated with the interface are found, and are compared with the theoretical expectations for a true heterojunction. The viability of ARP as a technique for probing heterojunction properties is discussed. In Part II, the discussion turns to crystalline metals. The (111) face of Au and Pt, and the (100) and (110) faces of Ag, are studied in detail using high-resolution variable-photon-energy ARP. Empirical dispersion relations are presented for each case, and compared with theory. Polarization and temperature dependent effects are analysed. Special attention is paid to final-state-induced spectral features, and consideration of both the energy and intensity behaviour of such features leads to the construction of a simple physical picture which both explains the observed phenomena and provides a justification for the use of a quasi-free-electron final state dispersion.

I. INTRODUCTION

One of the most fundamental concepts in solid state physics is that of the existence of dispersion relations which connect the energy of an electron to its wavevector. These relations, or energy bands, are the foundation on which an important part of the edifice of solid state physics is built.¹

Despite this, it has only been in the last decade, with the advent of the technique of photoelectron spectroscopy (*aka* PES or photoemission), that an experimental method has existed for the systematic and detailed study of the band structure of solids. All other methods, such as de Haas-van Alphen measurements, cyclotron resonance, Compton scattering, and positron annihilation, are capable of probing some aspects of the electronic structure, such as the shape of the Fermi surface or the nature of the momentum distribution, but none is capable of the simultaneous determination of binding energy and wavevector required to truly define the band structure.²

Indeed, even in the case of photoemission, it has only been in the last five years, with the introduction of angle-resolved techniques and the advent of synchrotron radiation sources, that such determinations have been possible. Previous to this period, PES measurements were typically performed in an angle-averaged mode with laboratory sources,

and while such an approach could provide much useful information, particularly concerning critical points and the density of states, it did not allow the determination of binding energies in arbitrary regions of the Brillouin zone.³ The inclusion of angular resolution and variable photon energies removed this last obstacle, providing complete momentum as well as energy resolution, in much the same way as measuring a differential instead of total cross section for tunable incident-particle energy more completely defines a scattering process.⁴

The experimental techniques involved in Angle-Resolved Photoemission (ARP) have been discussed at great length in the literature, and we shall not dwell on them here.⁵ Essentially, a suitably prepared single crystalline sample is irradiated with monochromatic radiation, typically in the photon energy range of 10 to 100 eV, and the photoejected electrons are kinetic-energy analyzed. Angular resolution is achieved by selecting for analysis only those electrons which originate within the desired solid angle. The kinetic energy is then related to the binding energy via the photoelectric equation

$$E_k = h\nu - E_B - \phi \quad , \quad (1)$$

where ϕ is the work function of the sample referenced to the spectrometer.⁶ Within a one-electron approach, these binding energies may be related to the microscopic quantum structure of the solid. The extraction of momentum information

is more complicated and requires the use of a suitable theoretical framework; this problem will be discussed in greater detail below.

The thrust of the research described in this thesis has been the use of ARP to elucidate dispersion relations in single crystalline solids. In the remainder of this introduction, we shall briefly review the concepts and formalism involved in such a study. Part I of this thesis will then describe work performed on semiconducting single crystals, which because of their complicated band structure and technological importance provide an interesting and challenging area for study. We shall in particular detail the results of two such investigations. In Chapter II, the conduction bands of GaAs will be mapped using variable photon energy ARP; this represents the first such mapping in semiconductors. Chapter III will then turn to the question of the electronic structure of a semiconductor-semiconductor heterojunction, presenting results suggesting the existence of states peculiar to such an interface, as well as describing their dispersion relations. In Part II, our attention will turn to the use of ARP to obtain dispersion relations in metals. Investigations of Pt(111) and Au(111) will be presented in Chapter IV, and of Ag(110) and Ag(100) in Chapter V. These results, in conjunction with those of other workers for analogous crystal faces of other 3d, 4d, and 5d metals, will enable us to make a strong case for the viability of ARP as a method for the

determination of accurate and detailed empirical band structures. We shall also discuss several other features observed in these studies, and describe how they can yield further insight into the nature of the photoemission process, as well as additional information on the electronic structure of metals.

A. The Direct Transition Model

A great deal of effort has been devoted to the theoretical description of ARP,⁷ including approaches based both on a one-electron picture and involving many-body effects as well.⁸⁻¹¹ Unlike the situation in gas phase photoemission, however, where many-body effects are quite important,¹² it is possible to satisfactorily interpret ARP from solids in a one-electron scheme, and this will be the approach adopted here.

Our analysis rests on two approximations. The first is that the binding energy of an electron as defined in Eq. (1) above is directly related to its eigenvalue in the Hartree-Fock sense (i.e., Koopman's theorem¹³). This will be valid as long as relaxation effects are small or constant. The second assumption involved is that the photoemission process occurs in three discrete steps:¹⁴ optical excitation, transport to the surface, and escape into the vacuum. In fact, the latter two steps are poorly understood, and usually neglected except for simple heuristic corrections; the majority

of the information of interest is contained in the actual optical excitation process, and we shall concentrate on it below. The seminal paper on the theoretical description of ARP is that of Mahan,⁸ and the following discussion is based largely on his work.

The essential quantity of interest is the photocurrent I , which is obtained by knowing the eigenfunction $\Psi(\vec{R})$ of the electron at a location \vec{R} far from the crystal:

$$I \sim \int d^3\vec{k}_i \operatorname{Im} \Psi^*(\vec{R}) \nabla_{\vec{R}} \Psi(\vec{R}) \quad . \quad (2)$$

The integration is over the manifold of initial states defined by the set of wavevectors $\{\vec{k}_i\}$ in reciprocal space. The problem then reduces to a determination of the wavefunction and evaluation of Eq. (2). For the former, recourse is made to scattering theory,⁴ which allows us to write

$$\Psi(\vec{R}) = \int d^3\vec{r}' G_0(\vec{R}, \vec{r}') \mathcal{H}' \psi_0(\vec{r}') \quad , \quad (3)$$

where G_0 is the free particle propagator, \mathcal{H}' the interaction Hamiltonian, taken to be¹⁵ $\vec{A} \cdot \vec{p} = \vec{A} \hat{\epsilon} \cdot \vec{p}$, and ψ_0 the electronic initial state Bloch functions.

Inside the crystal, for a one-particle approximation, the photocurrent for final state energy E is equivalent to an expression based on Fermi's golden rule:

$$I(E, h\nu, \vec{R}) \sim \int d^3\vec{k}_i \sum_{E_j(\vec{k}_i)} |\hat{\epsilon} \cdot \vec{R}|^2 \left| \langle \Psi(\vec{R}') | \nabla | \psi_0(\vec{R}') \rangle \right|^2 \\ \times \delta(E - E_j - h\nu) \quad . \quad (4)$$

The sum is over occupied initial states, and the initial-state eigenfunctions are Bloch waves. If we take $\Psi(\vec{R}')$ as a plane wave, with wavevector \vec{k} defining its propagation direction and wavelength, this equation reduces to

$$I \sim \int d^3k_1 \sum_{E_j} \delta(E - E_j - h\nu) |\vec{\epsilon} \cdot \vec{R}'|^2 \phi_j^2(\vec{k}) \times \left| \sum_{\vec{R}'} e^{i(\vec{K} - \vec{k}_1 - \vec{k}_\gamma) \cdot \vec{R}'} \right|^2 \quad (5)$$

where \vec{k}_γ is the photon momentum, and $\phi_j(\vec{k})$ the Fourier transform of the periodic part of the initial-state Bloch function, evaluated at \vec{k} . It then follows that there will be both momentum and energy constraints for photoexcitation, as given by

$$\begin{aligned} \vec{K} - \vec{k}_1 - \vec{k}_\gamma &= \vec{G} \\ E &= h\nu + E_j \end{aligned} \quad (6)$$

where \vec{G} is any reciprocal lattice vector; \vec{k}_γ is small and is usually ignored. Equations (6) define the requirements for a direct optical transition, and form the basis of the direct transition model.

The angular distribution of electrons inside the crystal follows from Eqs. (6). Using a free-electron dispersion relation for simplicity, we obtain

$$\frac{\hbar^2 K^2}{2m} = \frac{\hbar^2 |\vec{K} - \vec{G}|^2}{2m} + h\nu \quad (7)$$

which gives for the energy of the excited electron,

$$E = \frac{\hbar^2 K^2}{2m} = \frac{\Lambda^2}{4E_G \cos^2 \theta_0} \quad (8)$$

where $E_G = \hbar^2 G^2/2m$, $\Lambda = \hbar v + E_G$, and θ_0 is the angle between \vec{K} and \vec{G} . Thus, the energy of an electron depends only on θ_0 , and electrons of equal E will have equal θ_0 ; photoelectrons of equal energy form a conical distribution, centered about the associated G -vector. Such photoemission is called "primary cone emission." Since the crystal potential mixes states of different G , however, an excited electron with wavevector $\vec{k}_i + \vec{G} + \vec{G}'$ will also be in an eigenstate of the crystal. Its direction will then be different from a primary electron; such an excitation is called "secondary cone" emission.¹⁶ The coefficients of mixing will behave from first order perturbation theory as $[E(\vec{K}) - E(\vec{K} + \vec{G}')]^{-1}$, being largest for $\vec{G}'=0$; this implies that secondary emission should be a weak effect, and such is usually the case. These distributions extend outside the crystal as well, due to the presence of specular boundary conditions for the conservation of momentum across the vacuum-solid interface:

$$\begin{aligned} \vec{p}_{\parallel} &= \vec{K}_{\parallel} && \text{(primary emission)} \\ \vec{p}_{\parallel} &= \vec{K}_{\parallel} + \vec{G}'_{\parallel} && \text{(secondary emission)} \end{aligned} \quad (9)$$

From the above analysis, a simple picture arises for the correlation of ARP spectra with the band structure. If we take the final state (i.e., conduction) bands and state

them down in energy by $h\nu$, the intersections that will occur between them and the initial state bands will define the allowed transitions. Primary cones will result for final states with a significant group velocity along the detector direction (i.e., \vec{G}), while the secondary cones will result for the other transitions. These intersections also define the initial-state momentum. Alternatively, the combination of empirical binding energies and an appropriate choice of the final state - which in the simplest case may be just a plane-wave-like dispersion relation - allows the mapping of the initial state bands. An especially useful result obtains for photoemission normal to a particular crystal face. In this case, $\vec{k}_{\parallel} = 0$, and energy conservation is manifested in the relationship between \vec{k}_{\perp} and \vec{p}_{\perp} . Most importantly, no refraction can occur at the surface, and for primary emission, we will thus have initial states along the line in reciprocal space defined by the G-vector normal to the surface. For an appropriate choice of geometry, this enables the mapping of bands along high-symmetry lines in k-space.

B. Competing Mechanisms and the Breakdown of Direct Transitions

While the processes described above will in many cases account for the major features of an ARP spectrum, it is nevertheless true that such a spectrum will invariably contain other effects not predicted by a simple direct

transition model. In this section, we will briefly describe the major additional mechanisms which will be expected to play a role in the photoemission process, and indicate how the resulting additional structure can provide new insights into the electronic properties of the material under investigation.

1. Surface State Photoemission

The existence and characteristics of surface states have been topics of considerable theoretical interest in the current literature of both semiconductors and metals,¹⁷ and ARP provides a direct method for the investigation of such states. Their dispersion will be defined by the quantum number \vec{k}_{\parallel} in a two-dimensional surface Brillouin zone constructed from the three-dimensional zone by setting $k_{\perp} = 0$. The momentum is thus exactly characterized in an ARP experiment by the binding energy and geometry via¹⁸

$$p_{\parallel} = \left(\frac{2m}{\hbar} \right)^{\frac{1}{2}} (h\nu - E_B - \phi)^{\frac{1}{2}} \sin\theta \quad (10)$$

where ϕ is the work function and θ the angle between the surface normal and the electron propagation direction. Equation (10) allows the direct determination of surface dispersion relations from ARP data.

A great deal of work has been done investigating surface states by ARP, and we will only cite some reviews here.¹⁹ In this thesis, we will have occasion in Part II

to discuss surface states in more detail. In addition, a two-dimensional Brillouin zone may also be employed to describe states localized at an interface, and the approach described above may then be used to determine their dispersion relations. Chapter III will in large measure be concerned with such a study.

2. Polarization Effects

It is well known in atomic physics that the selection rules for an optical transition will depend on the polarization of the incident radiation; this result is a consequence of the transformation properties of the atomic wavefunctions and the interaction Hamiltonian under the point group of the atom.²⁰ While in solids the Bloch functions will transform under a space group, it is nevertheless true, as first discussed by Hermanson for materials described by a single space group,²¹ that group theory will prescribe selection rules in certain cases. The key requirement for such selection rules to exist is that the geometry be chosen to give a final state of definite symmetry at the detector; this is always the case for photoemission in a mirror plane of the crystal which contains the surface normal. Given such symmetry in the final state, one can then determine the allowed initial state symmetries, which will depend on the polarization of the incident radiation. It is customary to talk about two varieties of polarization in the ARP literature: "s-polarization," in which the

E-vector of the radiation is parallel to the crystal surface, and "p-polarization," in which it is not. The use of this definition for p-polarized light is actually somewhat unfortunate, as such a geometry is really a mixture of the two orthogonal basis polarizations, which are perpendicular and parallel to the surface; for fairly large angles of incidence, however, "p-polarized" light will be primarily one polarization and will show selection rule effects for that polarization.

There are several studies in the ARP literature using polarized radiation, for both semiconductors and metals.²² The work described in Chapter II serves as one example. We shall also have occasion in Chapter IV to consider these effects when we discuss Pt(111). For this metal, the Bloch functions include relativistic (spin-orbit) effects, and hence transform under a double space group; this somewhat complicates the analysis, but the selection rules may still be obtained from the character tables of the double group.²³ One more consequence of polarization is worth mentioning. For p-polarized light at near grazing incidence, an effect known as surface photoemission can occur,²⁴ in which the interaction of the photon's E-vector with the surface will result in significant photoemission intensity via indirect transitions. This effect is most commonly observed in lower-Z materials, and we will not have occasion to discuss it further.

3. Band-Gap Photoemission

The discussion in section A above was based on the assumption of a continuous itinerant final state for photoemission. In reality, however, there will be band gaps for conduction states, just as there are for valence states. In these gaps, the bulk final state will be exponentially damped (i.e., characterized by a complex wavevector), and photoemission will be allowed only if this state is close enough to the surface to couple with a plane wave in the vacuum. This band-gap photoemission has been reported in ARP studies of tungsten²⁵ and copper²⁶. It is still a matter of some controversy in the ARP literature as to exactly how spectra with final states in the gap are to be interpreted; in particular, whether one should expect to see dispersion, and whether direct transitions to a continued plane-wave-like final state, or one-dimensional density of states features, will prevail. In Chapters IV and V, we will discuss these questions in considerable detail, and develop a consistent physical framework for interpreting gap-photoemission.

4. Density of States Photoemission

While the direct transition model has achieved increasing acceptance in recent years, there is still some controversy regarding the extent to which density of states features will contribute to the photoemission spectrum.²⁷ In the case of metals, it is now well established that direct transitions will predominate to well over 100 eV photon energy at room temperature;²⁸ for semiconductors, however, as we will

indicate in Chapter II, this energy cutoff may be as much as a factor of four lower.

Two types of density of states features are commonly observed in ARP spectra. The first, known as one-dimensional (ODDOS), derive from critical points associated with the k-space symmetry line under study. Features associated with the total density of states (TDOS) may also occur. DOS features arise because of a breakdown in momentum conservation, and there are many mechanisms which can cause this.^{29,30} ODDOS features are generally considered to occur due to phonon-assisted indirect scattering or final-state momentum broadening, while TDOS features may arise from these processes, and from the effects of surface roughness or the use of high (x-ray) photon energies as well. We shall have some occasion to discuss DOS features in later chapters, but they are in fact more a hindrance than a help in using ARP results, and the experiments described here have been so designed as to minimize their presence.

5. Thermal Broadening

To the extent that electron-phonon scattering will occur during the photoemission process, we may expect the temperature, which determines the population of phonon modes, to play an important role in influencing the structure of an ARP spectrum. This effect has in fact been dramatically demonstrated in copper,³⁰ where heating can be shown to lead to a complete breakdown in direct transitions. The corollary

is of course that cooling will tend to diminish contributions from non-direct processes; the efficacy of such a procedure will depend both on the range of temperatures available and the Debye temperature of the material under investigation. For gold, as will be discussed in Chapter IV, the effects of cooling are quite dramatic. Changing the temperature also provides a way of discriminating features due to phonon-moderated indirect transitions from those involving temperature-independent mechanisms, and can also contribute to the quality of a spectrum via its effect on phonon processes which contribute to the inelastic background.³¹ Both of these topics will be considered in Chapter IV.

6. Momentum Broadening

The finite mean free path of photoelectrons implies, by a simple application of the Heisenberg uncertainty principle, that a certain amount of momentum broadening will occur in the final state.^{19a,28,31,32} For electrons propagating at an angle θ relative to the surface normal, one may roughly estimate³³ the uncertainty in K_{\parallel} as $\Delta K_{\parallel} \approx 4/\lambda \cos \theta$, where λ is the mean free path. For a photon energy of 30 eV, this will only represent ca. 5% of a typical Brillouin zone dimension, but by 130 eV such broadening can amount to as much as 20% of this distance. If the initial state bands show significant dispersion, a marked degradation in the energy resolution will result. Accordingly, it is preferable whenever possible

to work in the lowest photon energy range which allows accessing all the initial states desired. The work described in this thesis has accordingly been performed at photon energies under 35 eV.

7. Refraction

In the case of normal emission, the propagating photoelectron will penetrate the surface of the crystal and escape into the vacuum without suffering a change in direction; this occurs because K_{\parallel} is zero and the change in energy due to the work function is absorbed entirely by a change in the magnitude of \vec{K} . For non-normal emission, however, the conservation of the tangential component of the wavevector, in combination with that of energy, requires a bending of the electron as it escapes into vacuum.³³ This process considerably complicates the interpretation of ARP spectra, since knowledge of the final propagation direction outside the crystal no longer guarantees knowledge of that inside. While simple schemes exist for calculating the angular deviation³⁴, which may be as large as several degrees for emission significantly off-normal, there is at present no satisfactory method for accurately correcting for refraction. As a result, the precise mapping of bands requires the use of a normal emission geometry and variable photon energy; this is the approach which has been used in the work presented here.

REFERENCES

1. J.M.Ziman, Principles of the Theory of Solids, (University Press, Cambridge, 1972).
2. A.P.Cracknell and K.C.Wong, The Fermi Surface, (Clarendon Press, Oxford, 1973).
3. M.Cardona and L.Ley, eds., Photoemission in Solids I, (Springer-Verlag, Berlin, 1978).
4. L.I.Schiff, Quantum Mechanics, (McGraw-Hill, New York, 1968).
5. N.V.Smith, in Ref. 3; C.S.Fadley, J. Elect. Spect. Rel. Pheno. 5, 725 (1974); H.Ibach, ed, Electron Spectroscopy for Surface Analysis, (Springer-Verlag, Berlin, 1977).
6. The determination of absolute binding energies is a non-trivial problem of calibration, and has been discussed by M.F.Ebel, J. Elect. Spect. Rel. Pheno. 8, 213 (1976). Energies in solids may be references to the Fermi level, which avoids this problem.
7. G.D.Mahan, in L.Fiermans, J.Vennik, and W.Dekeyser, eds., Electron and Ion Spectroscopy of Solids, (Plenum Press, New York, 1977).
8. G.D.Mahan, Phys. Rev. B2, 4334 (1970).
9. J.B.Pendry, Surf. Sci. 57, 679 (1976).
10. W.Schaich and N.W.Ashcroft, Phys. Rev. B3, 2452 (1971).
11. C.Caroli, D.Lederer-Rozenblatt, B.Roulet, and D.Saint-James, Phys. Rev. B8, 4552 (1973).

12. L.S. Cederbaum and W. Domcke, *Adv. Chem. Phys.* 36, 205 (1977).
13. T. Koopmans, *Physica* 1, 104 (1933).
14. H.Y. Fan, *Phys. Rev.* 68, 43 (1945); W.R. Spicer, *Phys. Rev.* 112, 114 (1958); C.N. Berglund and W.E. Spicer, *Phys. Rev.* 136, A1030 (1964); W.F. Krowlikowski and W.E. Spicer, *Phys. Rev.* 185, 882 (1969).
15. There is, in fact, no gauge transformation in a solid which causes the $\vec{p} \cdot \vec{A}$ term to vanish, but it is common practice to ignore this complication. For a discussion of the vector potential in a solid, see K.L. Kliewer and R. Fuchs, *Phys. Rev.* 172, 607 (1968) and P.J. Feibelman, *Phys. Rev.* B12, 1319 (1975).
16. An alternate viewpoint of secondary emission is that the value of \vec{G}_{\parallel} added on escape represents a surface umklapp process. Accordingly, electrons propagating at an angle θ_0' in the crystal will scatter to an angle θ_0 which can coincide with the angle of a primary cone for a different G-vector.
17. J.A. Appelbaum and D.R. Hamann, *Rev. Mod. Phys.* 48, 479 (1976); G. Allan, in E.G. Derouane and A.A. Lucas, eds., Electronic Structure and Reactivity of Metal Surfaces, (Plenum Press, New York, 1976); F. Garcia-Moliner and F. Flores, *J. Phys.* C9, 1609 (1976).
18. E.O. Kane, *Phys. Rev. Lett.* 12, 97 (1964).

19. (a) B.Feuerbacher and R.F.Willis, *J. Phys.* C9, 169 (1976);
(b) J.W.Gadzuk, in E.G.Derouane and A.A.Lucas, eds.,
op. cit.; R.Gomer, ed., Interactions on Metal Surfaces,
(Springer-Verlag, Berlin, 1975).
20. M.Tinkham, Group Theory and Quantum Mechanics, (McGraw-Hill, New York, 1964).
21. J.Hermanson, *Solid State Comm.* 22, 9 (1977); N. V. Richardson, D.R. Lloyd, and C.M. Quinn, *J. Elect. Spect. Rel. Pheno.* 15, 177 (1979).
22. J.A.Knapp and G.J.Lapeyre, *Il Nuovo Cim.* 39B, 693 (1977); J.E.Rowe, G.Margaritondo, and H.Kasper, *Il Nuovo Cim.* 38B, 226 (1977).
23. R.J.Elliot, *Phys. Rev.* 96, 280 (1954); G. Dresselhaus, *Phys. Rev.* 100, 580 (1955).
24. K.L.Kliwer, *Phys. Rev.* B14, 1412 (1976) and *Phys. Rev.* B15, 3759 (1977).
25. N.E.Christensen and B.Feuerbacher, *Phys. Rev.* B10, 2349 (1974); B.Feuerbacher and N.E.Christensen, *Phys. Rev.* B10, 2373 (1974).
26. E.Dietz and F.J.Himpsel, *Solid State Comm.* 30, 235 (1979).
27. L.Ley, *J. Elect. Spect. Rel. Pheno.* 15, 329 (1979).
28. D.A.Shirley, J.Stohr, P.S.Wehtner, R.S.Williams, and G.Apai, *Physica Scripta* 17, 398 (1977).
29. P.J.Feibelman and D.E.Eastman, *Phys. Rev.* B10, 4932 (1974).
30. N.J.Shevchik, *J. Phys.* C, L555 (1977) and *Phys. Rev.* B16, 3428 (1977); R.S. Williams, P.S. Wehtner, J. Stohr, and

- D.A. Shirley, Phys. Rev. Lett. 39, 302 (1977).
31. J.M. Ballantyne, Phys. Rev. B6, 1436 (1972); B.L. Henke, J. Liesegang, and S.D. Smith, Phys. Rev. B19, 3004 (1979).
32. D.J. Spanjaard, D.W. Jepsen, and P.M. Marcus, Phys. Rev. B15, 1728 (1977).
33. R.S. Williams, Ph.D. Thesis, University of California, Berkeley, Lawrence Berkeley Laboratory Report LBL-7676 (May 1978).
34. R.S. Williams, P.S. Wehner, J. Stohr, and D.A. Shirley, Surf. Sci. 75, 215 (1978).

PART I.

SEMICONDUCTOR STUDIES

What am I now to take of all this scarcity ?

Terence, *Phormia* , i.3,14

II. FINAL-STATE BANDS IN GaAs*

Photoelectron spectroscopy has proven to be of great utility in the study of the electronic properties of solids. Recently, angle-resolved photoemission (ARP), together with the direct-transition model, has become well established as a method for elucidating the band structures of metals.¹ In the case of semiconductors, however, the detailed relationship of the PES spectra and the band structure is much less well understood, and until now most studies of such materials have focused on the elucidation of their integrated densities of states,² surface states,^{3,4} and interactions with metallic, semiconducting, or insulating overlayer materials.⁵ The interpretation of ARP data for three-dimensional solids, such as zincblende and rocksalt structure conductors, has primarily involved two opposing viewpoints: the one-dimensional density of states (ODDOS) approach and the direct transition model (DTM). Grandke, *et al.*⁶ analyzed spectra at 21.2 eV photon energy for PbS using the former approach, and concluded that it explained the features observed; more recently, Thiry, *et al.*⁷ have studied PbSe for variable photon energies, and have shown the viability of the ODDOS approach for mapping bulk bands. On the other hand, Rogers and Fong⁸ used the DTM successfully to interpret GaAs(110) photoemission results for $h\nu \leq 8$ eV, and Knapp, *et al.*⁹ have reported using the DTM to 16 eV for this material. Because of the relative complexity of the final-

state band structure, however, it has until now been difficult to use ARP data, in an analytical sense, as a probe of the bulk electronic structures of semiconductors; that is, using the spectra to derive, or at least to adjust, dispersion relations, rather than simply using a theoretical band structure to explain the spectra. We shall present here conduction bands for GaAs(110), which were derived by a rather simple analysis. We also present evidence for the ODDOS mechanism at higher photon energies.

A. Experimental

The (110) cleavage face of GaAs was chosen for these studies, as its valence band structure is well known¹⁰⁻¹³ and it has been extensively characterized by other methods. Spectra were taken at photon energies up to 28 eV using synchrotron radiation from the SPEAR storage ring at Stanford Synchrotron Radiation Laboratory, using a cylindrical mirror analyzer modified for angle-resolved studies, with an energy resolution of 0.07 eV. The sample was an n-type GaAs(110) crystal cleaved *in situ*, and mounted on a manipulator that allowed full polar (θ) and azimuthal (ϕ) rotations; the base pressure was in the 10^{-10} torr range. Spectra were taken for several combinations of θ and ϕ ; the results presented here are for normal emission ($\theta = 0$), with azimuthal orientations corresponding to the [001] ($\phi = 0^\circ$) and [110] ($\phi = 90^\circ$) directions

in the bulk Brillouin zone being in the plane of the polarization vector. The detector lay in the plane of the polarization vector; the angle between the photon beam and the detector acceptance axis was fixed at 62.7° . Spectra were taken for two separate samples, and were reproducible; angular alignment was achieved using a He-Ne laser. All binding energies were referenced to the experimental valence band maximum at Γ , taken from the high energy spectra; the spectra were aligned to a constant Fermi level as determined from a gold foil in electrical contact with the sample.

B. Direct Transition Analysis

In Figure 1 we present spectra in the photon energy range 12-20 eV, for both azimuthal orientations. As shown by Lapeyre and coworkers,¹³ the polarized nature of the incident radiation determines selection rules for the spectra. In this case, only Σ_1 final states are allowed for normal emission, and the orientation of the polarization vector relative to the sample mirror plane implies that for $\phi=90^\circ$, all initial states are allowed, while for $\phi=0^\circ$ the highest valence band A (we label the three highest initial state bands A-C, in order of increasing binding energy), of Σ_2 symmetry, will not be observed. All the features in the spectra seem to be bulk-like, except for the shoulder at 0.8 eV binding energy (BE) for $h\nu=12$ eV. This peak is also observed at 0.6 eV BE for $h\nu=9$ eV, and at 0.7 eV BE for

$h\nu = 7$ eV; in the latter two cases, no direct transitions are predicted within 1 eV of this BE, and we accordingly assign the feature as a surface state. While a surface state is not predicted at $\bar{\Gamma}$,¹² the finite angular resolution of the analyzer would allow the observation of surface states nearby.

We have chosen to analyze these spectra by using them to map the allowed final states. The valence bands given by Chelikowsky¹⁰ were chosen, as his C band BE along the K-X direction was in better agreement with our data than that of Pandey and Phillips¹¹ (PP). The initial states are shown in Figure 2. Our procedure was essentially as follows: By comparing the PP band structure with a free electron band structure, it was possible as a first approximation to assign a projection of the group velocity along the [110] direction for each of the conduction bands (Figure 3). We note that for most of the real bands, several free-electron bands will be dominant, one in each segment through the Brillouin zone, because the bands admix and invert several times in going from Γ to X; accordingly, each final state band was divided into its free-electron-like constituents. Most of the final state bands under consideration arose from five G vectors and their associated energy-degenerate partners: (220), (1 $\bar{1}$ 1), ($\bar{1}\bar{1}\bar{1}$), (0 $\bar{2}$ 0), and (02 $\bar{2}$). All of these free electron bands have [110] projections of 60% or greater. The remaining PP final states had associated projections of one-third or less

and were therefore disallowed because of the angle-resolved nature of the experiment. Using this selected group of PP final states, the energies of all possible direct transitions were calculated. These transitions were labeled according to both their initial state and the free-electron-like component of the final state. Transitions falling on a final-state inflection point were treated separately. By comparing these assignments to the spectra, it was possible to unambiguously assign empirical transition energies to roughly 50% of the transitions. These energies were then used to map the accessible final state bands; finally, these empirical bands were then used to predict the balance of the transitions. All peaks were accounted for in this manner.

Such an approach is iterative, and its success depends on starting with a rather good idea of the final-state band structure. We emphasize that our analysis was conservative, and only relatively small adjustments were made in the final-state bands. Where several transitions occurred under a single peak, no empirical energy was incorporated into the conduction band structure unless additional analysis, such as following trends in given initial to final-state transitions, gave a way of making an unambiguous assignment. In a few cases, bands with the proper [110] projection were not observed; this was attributable either to the photon energy range employed or masking of the associated transition by other features. Consistency was maintained at all times;

in particular, a transition from a given initial state to a given (k) region of a final state was assigned for all photon energies where it was predicted theoretically, unless it was clearly associated with a peak that grew in or out with increasing photon energy. For a very few transitions, which fell in gaps in the spectra, it was necessary to assume that they were disallowed due to cross-section effects; again, such transitions were discarded in all spectra to ensure consistency. Polarization effects were also utilized whenever possible, and in particular, it was possible by calculating difference spectra to assign some A band transitions in the $\phi = 90^\circ$ spectra.

The results of this mapping are shown in Figure 4, where they are compared to the theoretical band structure of PP. We have shifted the PP bands down by 0.5 eV to give the best overall agreement, and in fact this shift is necessary if the PP final state bands are to predict all the major features in the spectra. We note that one Σ_2 final state band is observed (band 2). This arises from the finite angular resolution of the spectrometer, coupled with the fact that this band has a deep minimum, and concomitant high density of states, midway along the Γ -K line. The associated peaks are at 3.7, 4.4, and 5.2 eV BE for photon energies of 12, 13, and 14 eV, respectively, and correspond to transitions from the C initial state. The peak at 4.4 eV for $h\nu = 14$ eV comes from the minimum in band B near K, and indicates that

the theoretical initial state band structure is in error here by roughly 0.2 eV; no attempt was made to correct for this in our analysis. Broadening due to the finite mean free path may be estimated; for an escape depth¹⁴ of 15 Å, the k-broadening is roughly 1/16 of the Γ -X distance.¹⁵ The final energy uncertainty depends in each case on the nature and shape of the peak involved, but we estimate it at ± 0.2 eV in most cases; of course, any errors in the initial state band structure will also contribute.

C. Onset of Density of States Features

Figure 5 shows the evolution of the ARP spectra for higher proton energies, $h\nu = 22-28$ eV. Only the $\phi = 90^\circ$ spectra are shown; those for $\phi = 0^\circ$ were similar. Without a theoretical final state band structure we are unable at present to make a quantitative interpretation of these spectra. It seems evident, however, that a new photoemission mechanism is becoming dominant in this energy range. We note in particular that the spectra are still evolving up to $h\nu \cong 25$ eV, but that they have settled for higher energies into a structure that does not vary markedly with photon energy.

The most probable explanation for this behavior is the onset of a ODDOS regime. At electron kinetic energies somewhat above the plasmon threshold, electron mean free paths fall to very low values in metals and semiconductors. In fact, Pianetta¹⁶ found an electron mean free path in GaAs

of $6 \pm 1.5 \text{ \AA}$ at 40 eV kinetic energy. This would imply that our highest energy spectra are dominated by the first two GaAs atomic layers. Moreover, the consequent broadening in k_{\perp} implies effective non-conservation of this quantum number and sampling through the entire Brillouin zone in a direction normal to the surface: i.e., a ODDOS sampling. We note that Thiry et al.⁷ have observed ODDOS behavior in PbSe at $h\nu = 35$ eV photon energy and have tentatively interpreted it in this way, using the ODDOS to identify the critical points and map the valence band structure. To test this interpretation for the GaAs case, we have computed the ODDOS for GaAs along Γ KX and compared it with our high-energy spectra in Figure 6. The agreement is excellent, especially when we note that the s to p photoemission cross section ratio is very small at these energies, effectively suppressing the more tightly bound bands. Thus, the evidence is strong that a transition occurs between $h\nu = 20$ eV and $h\nu = 30$ eV from the direct transition mechanism to ODDOS behavior in photoemission from GaAs.

Two caveats are necessary, both of a generic nature and not specific to GaAs. First, a strictly logical approach would require that the direct-transition model be shown incapable of interpreting the high-energy spectra. This would be difficult in general as the final state bands become more numerous at high energies, and it is not possible at this time because we do not have theoretical high-energy bands.

It is very unlikely that our high-energy spectra can be reconciled with the DTM, since this would require the final states to evolve into a semi-continuum over this rather small energy range. The second caveat is simply that the transition from the DTM to ODDOS behavior with photon energy is not perfectly sharp, and one may expect some evidence of both at higher and lower energies. It is an obvious, but often neglected, fact that ARP spectra usually contain some spectral area that is not accounted for by the photoemission mechanism that dominates the spectra.

In conclusion, we have shown that it is possible by a simple analysis to map selected conduction bands in GaAs using ARP in the photon energy regime where the DTM is valid. For higher photon energies, the ODDOS is seen to account for the observed spectral features. It seems likely that such a two regime approach will account for the ARP spectra of other semiconductors as well, and that it should be possible to understand photoemission from three-dimensional solids in this framework.

REFERENCES

*This chapter appeared in part as "Mapping of Conduction Bands in GaAs," K.A. Mills, D. Denley, P. Perfetti, and D.A. Shirley, Solid State Comm. 30, 743 (1979).

1. See Chapters IV and V of this thesis for a complete discussion of the DTM in metals.
2. L. Ley, R.A. Pollak, F.R. McFeely, S.P. Kowalczyk, and D.A. Shirley, Phys. Rev. B9, 600 (1974); D.E. Eastman, W.D. Grobman, and J.L. Freeouf, Phys. Rev. B12, 4405 (1975).
3. J.A. Knapp and G.J. Lapeyre, J. Vac. Sci. Tech. 13, 757 (1976).
4. G.P. Williams, R.J. Smith, and G.J. Lapeyre, private communication.
5. P.E. Gregory and W.E. Spicer, Phys. Rev. B12, 2370 (1975); W.E. Spicer, P. Pianetta, I. Lindau, and P.W. Chye, J. Vac. Sci. Tech. 14, 885 (1977); P. Perfetti, D.A. Denley, K.A. Mills, and D.A. Shirley, Appl. Phys. Lett. 33, 667 (1978).
6. T. Grandke, L. Ley, and M. Cardona, Phys. Rev. Lett. 38, 1033 (1977); L. Ley, J. Elect. Spect. Rel. Pheno. 15, 329 (1979).
7. P. Thiry, R. Pinchaux, G. Martinez, Y. Petroff, J. Lecante, J. Paigne, Y. Ballu, C. Guillot, and D. Spanjaard, Solid State Comm. 27, 99 (1978).
8. D.L. Rogers and C.Y. Fong, Phys. Rev. Lett. 34, 660 (1975).

9. J.A.Knapp, D.E.Eastman, K.C.Pandey, and F.Patella, Bull. Am. Phys. Soc. 23, 399 (1978).
10. J.R.Chelikowsky, Ph.D. Thesis, University of California, Berkeley, LBL Rpt. LBL-3962 (Sept. 1975); J.R. Chelikowsky and M.L. Cohen, Phys. Rev. B14, 556 (1976).
11. See Ref. 13 for the Γ -K-X band structure; the original calculations are in K.C.Pandey and J.C.Phillips, Phys. Rev. B9, 1552 (1974), *loc. cit.*, 1560.
12. D.J.Chadi, Phys. Rev. B18, 1800 (1978).
13. J.A.Knapp and G.J.Lapeyre, Il Nuovo Cim. 39B, 693 (1977).
14. W.E.Spicer, J.S.Johannessen, and Y.E.Strausser, Varian Report VR-98, p.14; I. Lindau and W.E. Spicer, J. Elect. Spect. Rel. Pheno. 3, 409 (1974).
15. D.J.Spanjaard, D.W.Jepsen, and P.M.Marcus, Phys. Rev. B15, 1728 (1977).
16. Piero A. Pianetta, Ph.D. Thesis, Stanford University (1977), Stanford Synchrotron Radiation Laboratory Report 77/17, p.127.
17. Recent studies by Eastman and coworkers (T.C. Chiang, J.A. Knapp, D.E. Eastman, and M. Aono, to be published) for GaAs (110) using photon energies of up to 100 eV have indicated that a direct transition mechanism is suitable for interpreting the spectra over this entire energy range, and that the lack of evolution in the spectra for $h\nu \geq 26$ eV observed here may be explained in terms of the DTM if lifetime and surface umklapp effects are taken into account. Such an interpretation is not at variance with the

results presented here; their spectra are identical to ours, and the processes they invoke would give behaviour identical to that due to an ODDOS mechanism. In addition, the reestablishment of dispersion in their spectra for $h\nu \geq 45\text{eV}$ may also be attributed to an increase in the electronic mean-free-path, which would produce a changeover from ODDOS to DTM behaviour.

FIGURE CAPTIONS

- Fig. 1. Spectra in the photon energy range 12-20 eV for normal emission and both azimuthal orientations.
- Fig. 2. Band structure of GaAs from Ref. 10.
- Fig. 3. Free-electron band structure along Γ -K-X for GaAs. The right-hand side shows the G-vectors associated with each band and the left-hand side the projection of the band's group velocity on the [110] direction.
- Fig. 4. Empirical and theoretical conduction bands for GaAs(110). Portions of bands 5, 6, and 7 are not observed for the reasons discussed in the text. Dashed lines indicate a (110) projection of less than one-third for the group velocity.
- Fig. 5. Spectra at normal emission for the photon energy range 22-28 eV.
- Fig. 6. ODDOS compared to spectra at 26 and 28 eV photon energy. Note that the ODDOS should be broadened and corrected for cross section effects to allow a direct comparison with experiment. The feature at ca. 11-13 eV binding energy is a constant kinetic energy peak associated with structure in the final state bands.

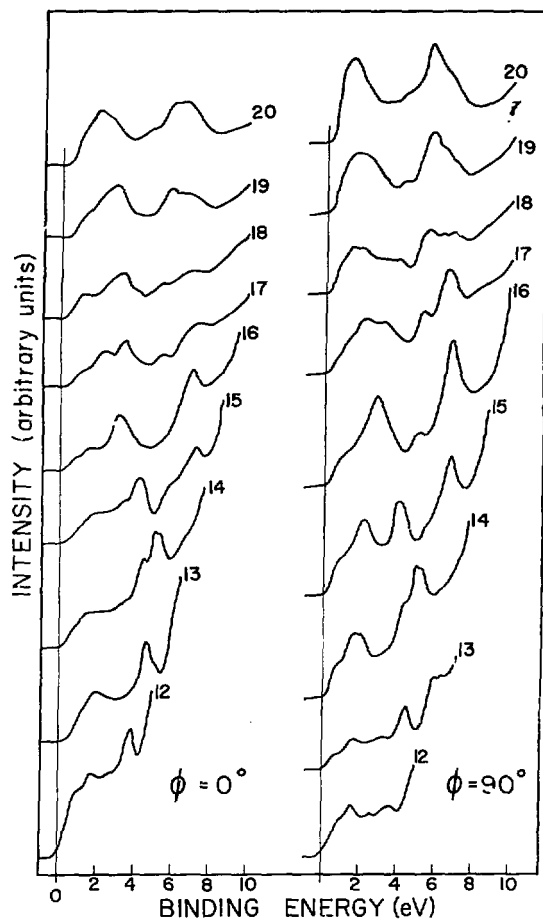


Fig. 1

XBL 787-9774

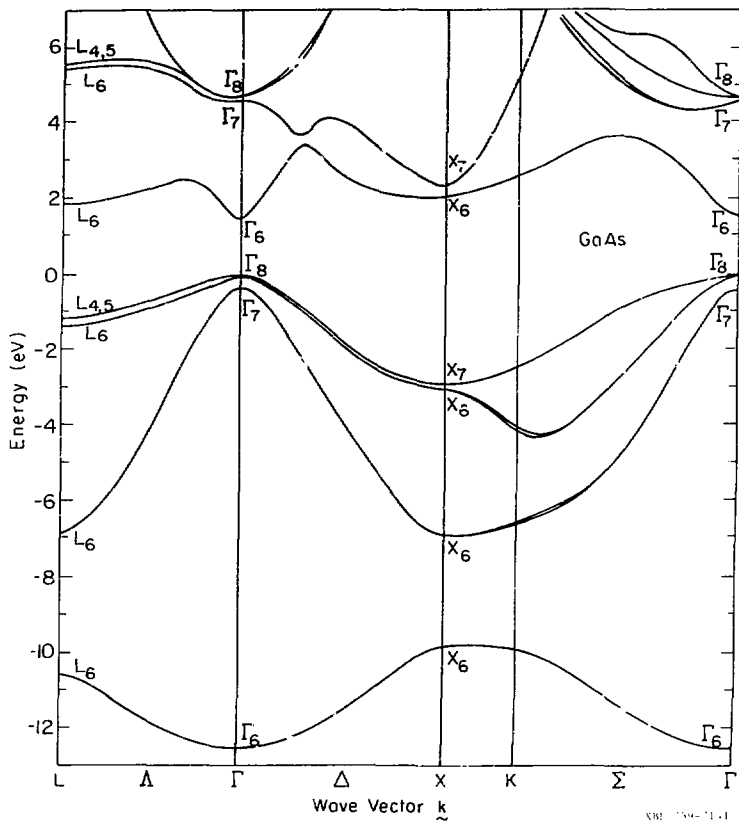


Fig. 2

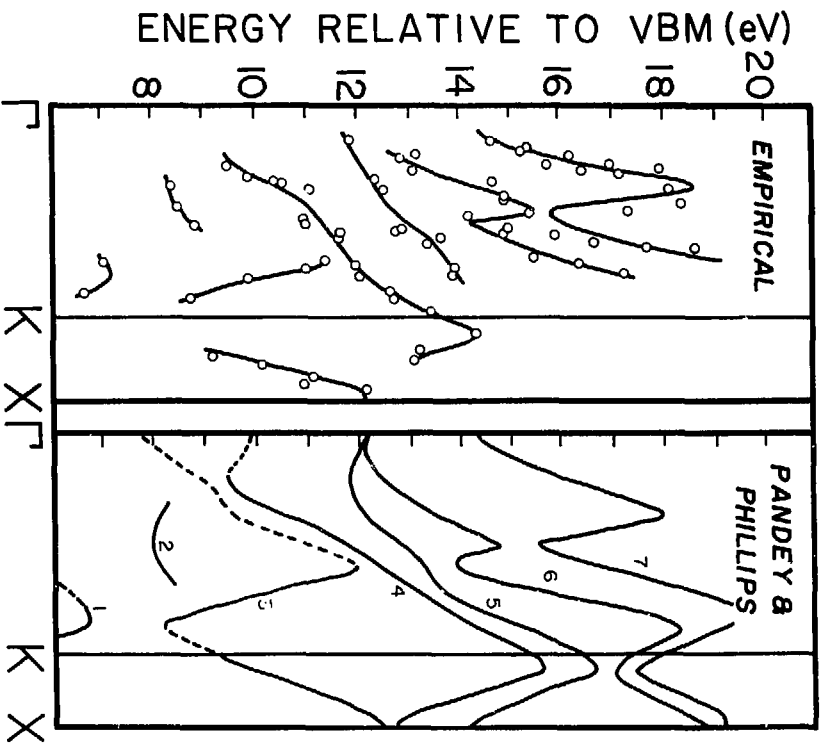


Fig. 4

XBL 787-9773

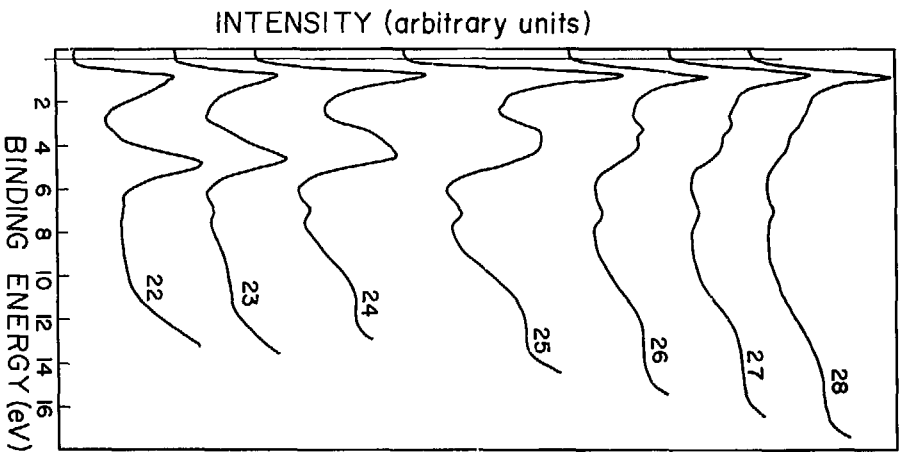


Fig. 5

XBL 787-9771

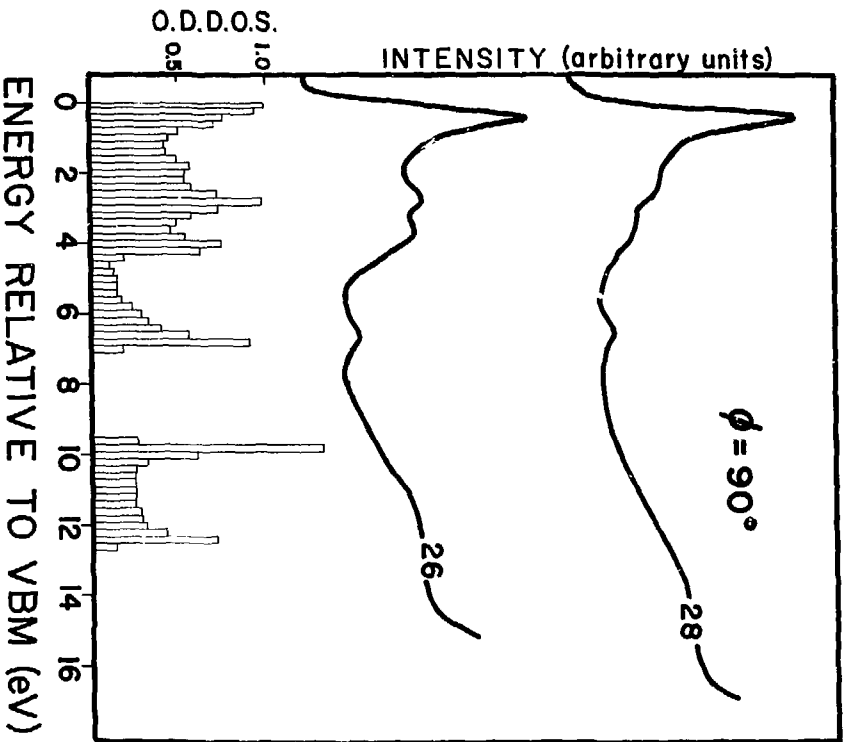


Fig. 6

XBL 787-9772

III. INTERFACE STATES IN GaAs/Ge*

The nature of the electronic structure of metal-semiconductor and semiconductor-semiconductor interfaces, and the process by which very thin films evolve toward the limit of two bulk materials joined at an interface, are of considerable scientific and technological interest. It has only been in the last few years, however, that microscopically sensitive techniques, such as angle-integrated photoemission,^{1,2} partial yield spectroscopy,³ and electron energy-loss spectroscopy⁴ have been utilized for studying the growth of metal films on semiconductors. Until now, these studies have been concerned primarily with the elucidation of general interface electronic properties such as band discontinuities.

Recently, we have found that angle-resolved photoemission (ARP) is a useful technique for studying discontinuities in semiconductor-semiconductor heterojunctions.⁵ We present here results of experiments which show that ARP may be used to more fully elucidate the detailed evolution of electronic structure in the initial stages of interface formation. In particular, we have found a number of features, some of which correspond to recent calculations of interface states.⁶ These features follow regular trends as successively greater amounts of Ge are deposited.

A. Experimental

The experimental apparatus has been described elsewhere.^{5,7} ARP spectra were taken at 21.2 eV (He I) photon energy for an n-type GaAs(110) single crystal cleaved *in situ*, using a CMA with an energy resolution of 0.07 eV; the sample orientation was fixed, following cleavage along the $\bar{\Gamma}\bar{X}'$ direction, by laser autocollimation. Successive layers of Ge were produced by evaporative deposition, with the substrate held at the epitaxial growth temperature⁸ of 350°C. Coverage was determined by calibrating the oven with a piezoelectric thickness monitor, with one monolayer defined¹ as 8.85×10^{14} atoms/cm²; the base pressure in the chamber was 2×10^{-10} torr. Spectra were taken as a function of θ , the polar angle from the surface normal, for azimuths corresponding to electron wavevectors along $\bar{\Gamma}\bar{X}$ ($\phi = 0^\circ$) and $\bar{\Gamma}\bar{X}'$ ($\phi = 90^\circ$) in the surface Brillouin zone (SBZ); the geometry is summarized in Figure 1.

B. Results for Low Coverage

A detailed analysis of GaAs photoemission was given in Chapter II of this thesis, and we shall review it only briefly here, as a basis for discussing the interface states. Most of the structure is associated with bulk transitions. At normal emission, all the peaks may be accounted for by the use of existing band structures^{9,10} and a direct transition model, except for the peak at ca. 13 eV. This latter feature, which is almost dispersionless with θ , was found to

be cleavage-dependent, and was observed to disappear for heavy Ge coverage. It occurs in a bulk band gap for GaAs. Accordingly, we attribute it to a new, deeply bound surface state in GaAs. No such state has been predicted for $\bar{\Gamma}\bar{X}$, although Chadi¹¹ has predicted a state at ca. 11.2 eV between \bar{M} and \bar{X} , and recent self-consistent calculations¹² show a surface resonance not yet split off the bulk bands at 11.5 eV.

Spectra are presented in Figure 2 for a series of evaporations corresponding to submonolayer coverages of Ge. Here, the electrons are emitted with the parallel component of their wavevector (\vec{k}_{\parallel}) oriented along the $\bar{\Gamma}\bar{X}$ line in the SBZ. The primary features are labeled one through four. Several phenomena are observed upon overlayer formation. The gap between the surface state 1 at 1.1 eV and the bulk peak 2 at 2.3 eV is seen to fill in; in addition, there is an apparent broadening of the latter feature and of peak 4 at 6.4 eV for evaporation 1 (E1). Apparent broadening in peak 2 also occurs, but has decreased by E2, as has that for peak 4 by E3.

These features are admittedly subtle. To better explicate them, we have calculated difference spectra, presented in Figures 3 and 4 for the various evaporations relative to the clean substrate. These spectra clearly show a loss in strength for the most weakly bound states. Such behavior is frequently observed in ARP spectra of adsorbate-

substrate systems, and is attributable to a transfer of intensity toward higher binding energy. In addition, several generally sharp features appear; they are summarized in Figure 5. The features are found to fit one of two cases for the location of at least some of their associated $(E_B, \vec{k}_{||})$ paired values: (1) in a region which is calculated to be forbidden to itinerant (bulk-like) states, or (2) within or at the edge of a region in which itinerant states are allowed. The first case is necessary for the formation of a truly localized state, while the second is typical for the occurrence of resonances.¹³ In the present experiment, all features falling above 7 eV are found to persist in the region of itinerant states, regardless of whether they can be found in gaps or not. For case (1), this is shown by features C for the $\bar{\Gamma}\bar{X}$ azimuth and E, F, and G for the $\bar{\Gamma}\bar{X}'$ azimuth, all of which penetrate from a gap into the bulk-forbidden region. The features D and H are noteworthy in that they fall in the ionic gap of GaAs. The effect on the surface of the Ge deposition, in the limit of a thick overlayer, will be to partially close the gap at \bar{X}' , and completely close it at \bar{X} . This will prevent the formation of localized states, and it is therefore consistent that D (and to a degree H) is strongly damped for greater depositions; in fact, feature D has disappeared by evaporation 3. All other features are persistent, and in particular the feature C agrees with the prediction of a "Ge-As bond" state (B_1) by Pickett, et al.⁶ at

3.64 eV. The feature F can correspond to either B_1 or P_1 of the above calculations, while feature E might be a resonant precursor of B_2 or P_2 . Feature G does not correspond closely to any predicted states.

Features corresponding to the second case are peaks A and B for the $\bar{\Gamma}\bar{X}$ azimuth. The feature B is found at mid-band and is of uncertain origin. The nature of the feature A, on the other hand, strongly suggests that it too is a resonant precursor for the interface state B_2 , analogous to feature E. One can trace the center of gravity of features A and E through the successive evaporations (Figure 6). In fact, evolution is found toward the main gap, with the trend being stronger for the E state.

C. Results for Higher Coverages

In order to pursue the effects described above, a second experiment was initiated with a new sample. Three evaporations were conducted, the first of these at a coverage which attempted to reproduce E3 in section B above, and the last two for 0.6 and 1.0 monolayers.

Comparison of the results for the two 0.3 monolayer coverages showed excellent agreement for the $\bar{\Gamma}\bar{X}$ direction and generally good agreement along $\bar{\Gamma}\bar{X}'$ with the exception of the highest ("E") feature, which was found to occur at ca. 0.5 eV higher binding energy for the second experiment. The explanation for this is unclear, and in fact this feature

appeared for the two subsequent evaporations at lower binding energy. In general, both the standard and difference spectra were of poorer quality in the second experiment, which leads to the supposition that the cleave obtained was inferior. Accordingly, while we feel these results worthy of discussion, they are quantitatively only tentative at best.

In Figures 7 through 11, we present plots of the features observed for the three evaporations of section B, and the final two evaporations (called E4 and E5 here) of the second experiment. Points worthy of note are the following. First, the states in the ionic gap are seen to have essentially vanished by 0.6 monolayers. Second, while there does seem to be a net trend along both directions for evolution into the gaps with increasing coverage, it is nevertheless clear that convergence with theory is not close, even at 1.0 monolayer. That these states are still penetrating into the bulk-forbidden regions of the zone seems to indicate that one monolayer coverage is not sufficient to describe a true interface. Unfortunately, the use of ultraviolet-energy ARP for coverages much larger than these is precluded by the small electron mean-free-path in this photon energy range. Conceivably, utilization of x-ray energies (where mean free paths may be as high as 50 Å) could overcome this problem, but the related breakdown of direct transitions would provide substantial new complications of its own. It seems then, that while ARP experiments can yield valuable insight into the initial

stages of interface formation, a new technique will need to be found if these interfaces are to be probed in the true heterojunction limit.

REFERENCES

- *Based in part on the paper, "Electronic Structure in GaAs/Ge Through Angle-Resolved Photoemission," D.Denley, K.A.Mills, P.Perfetti, and D.A.Shirley, *J. Vac. Sci. Tech.* 16, xxx (1979).
1. P.E.Gregory and W.E.Spicer, *Phys. Rev.* B12, 2370 (1975).
 2. G.Margaritondo, J.E.Rowe, and S.B.Christman, *Phys. Rev.* B14, 5396 (1976).
 3. W.Gudat and D.E.Eastman, *J. Vac. Sci. Tech.* 13, 831 (1976).
 4. J.E.Rowe, S.B.Christman, and G.Margaritondo, *Phys. Rev. Lett.* 35, 1971 (1975).
 5. P.Perfetti, D.R.Denley, K.A.Mills, and D.A.Shirley, *Appl. Phys. Lett.* 33, 667 (1978).
 6. W.E.Pickett, S.G.Louie, and M.L.Cohen, *Phys. Rev.* B17, 815 (1978).
 7. J.Stöhr, G.Apai, P.S.Wehtner, F.R.McFeely, R.S.Williams, and D.A.Shirley, *Phys. Rev.* B14, 5144 (1976).
 8. R.S.Bauer and J.C.McMenamin, *J. Vac. Sci. Techn.* 15, 1444 (1978).
 9. J.R.Chelikowsky, Ph.D. Thesis, University of California, Berkeley, Lawrence Berkeley Laboratory Report LBL-3962 (1975).
 10. J.A.Knapp and G.J.Lapeyre, *Il Nuovo Cim.* 39B, 693 (1977).
 11. D.J.Chadi, *Phys. Rev.* B18, 1800 (1978).
 12. J.R.Chelikowsky, private communication.
 13. B.Feuerbacher and R.F.Willis, *J. Phys.* C9, 169 (1976).

FIGURE CAPTIONS

- Fig. 1. Experimental geometry and surface Brillouin zone for GaAs.
- Fig. 2. Selected spectra for $k_{\parallel}^{\rightarrow}$ along $\bar{\Gamma}\bar{X}$ as a function of Ge coverage. Binding energies are referred to the valence band maximum at Γ .
- Fig. 3. Selected difference spectra for the $\bar{\Gamma}\bar{X}$ direction in the SBZ.
- Fig. 4. Selected difference spectra for the $\bar{\Gamma}\bar{X}'$ direction in the SBZ.
- Fig. 5. Observed ARP features and projected surface band structure for GaAs/Ge (after Ref. 6). Cross-hatched areas are GaAs bulk-forbidden regions. Interface states are labeled with the notation of Pickett, et al., and the features in Figures 3 and 4 are labeled as A through H. Peaks are plotted from data for all evaporations of section B, but not all data is shown; in some cases, peak positions were identical for successive evaporations.
- Fig. 6. Binding energy shift for peaks A and B as a function of Ge coverage. Each point represents the mean value of the set of points common to these features for each evaporation.
- Fig. 7. Observed ARP features for E1 (0.06 monolayers) of the first experiment.

- Fig. 8. Observed ARP features for E2 (0.12 monolayers) of the first experiment.
- Fig. 9. Observed ARP features for E3 (0.26 monolayers) of the first experiment.
- Fig. 10. Observed ARP features for E4 (0.60 monolayers), derived from the second evaporation in the experiment of section C.
- Fig. 11. Observed ARP features for E5 (1.0 monolayers), from the third evaporation in section C.

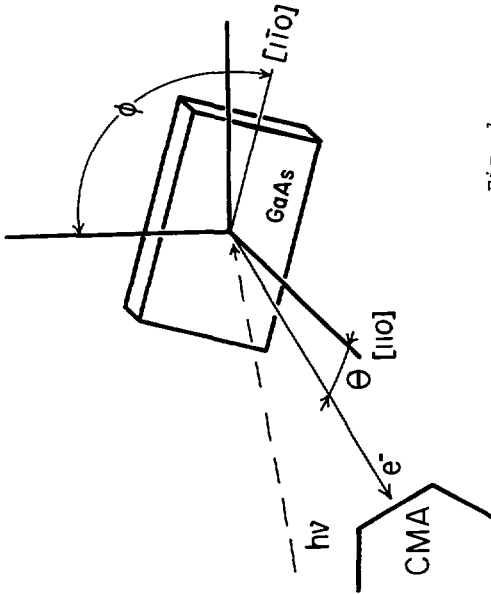
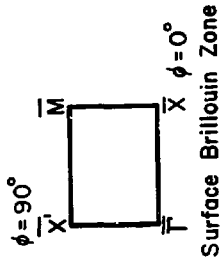
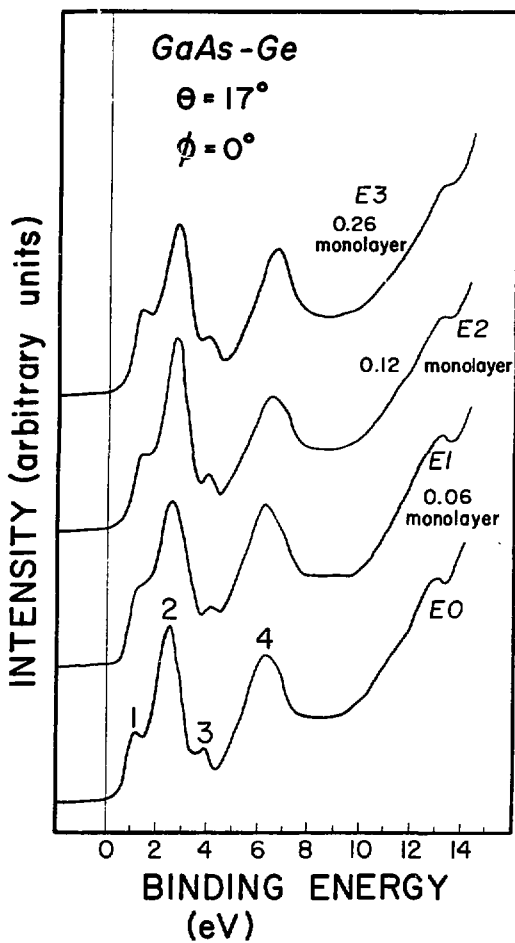


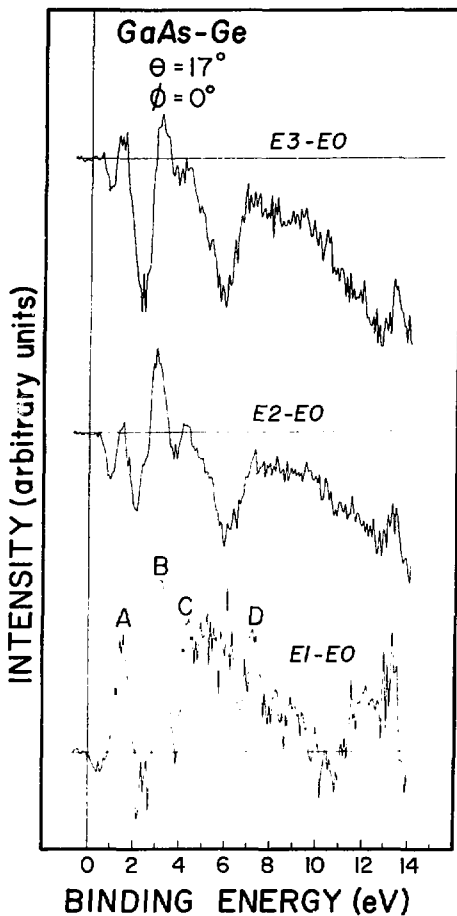
Fig. 1

XBL 792-8386



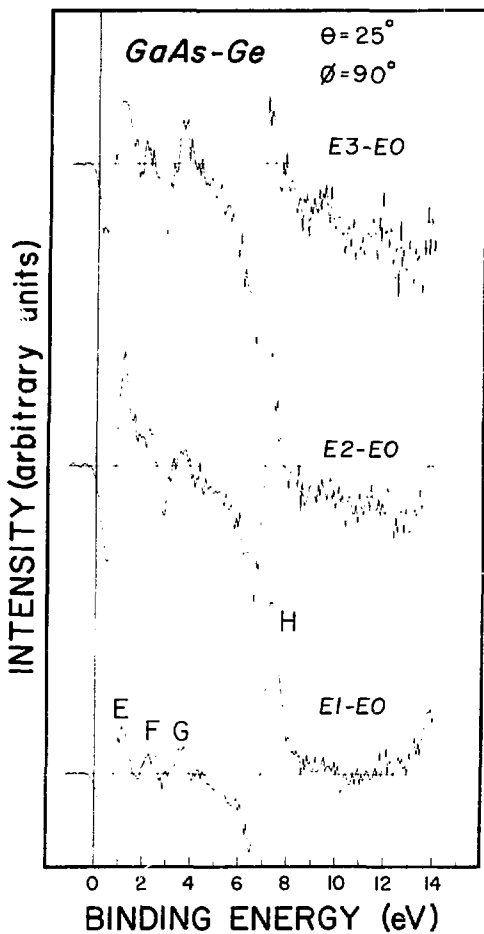
XBL 791-8087

Fig. 2



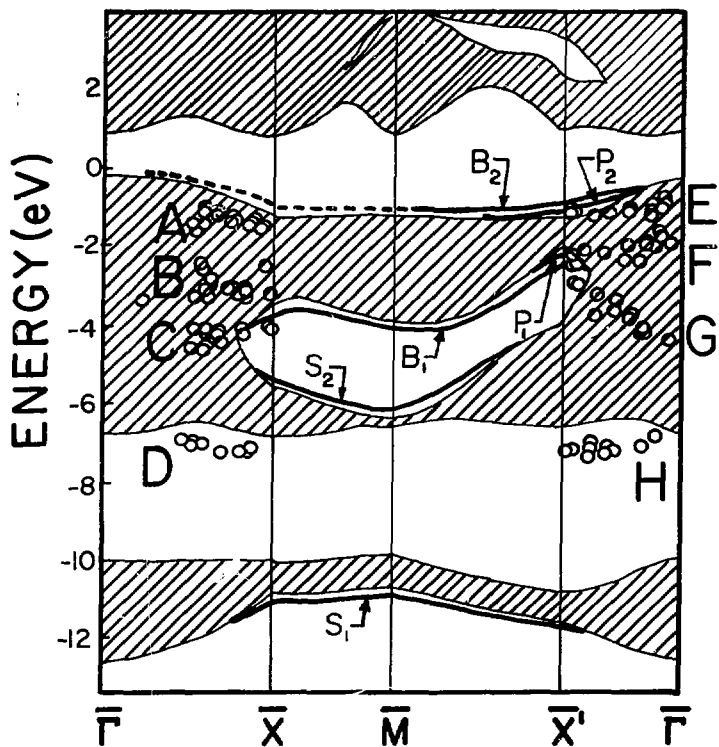
XBL 791-8088

Fig. 3



XBL 791-8094

Fig. 4



XBL 792-8387

Fig. 5

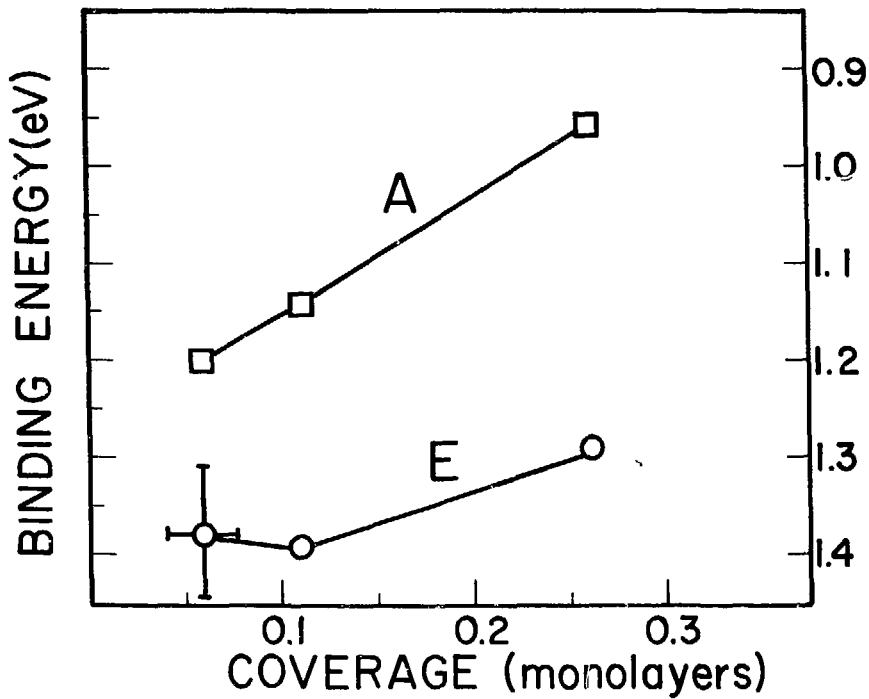
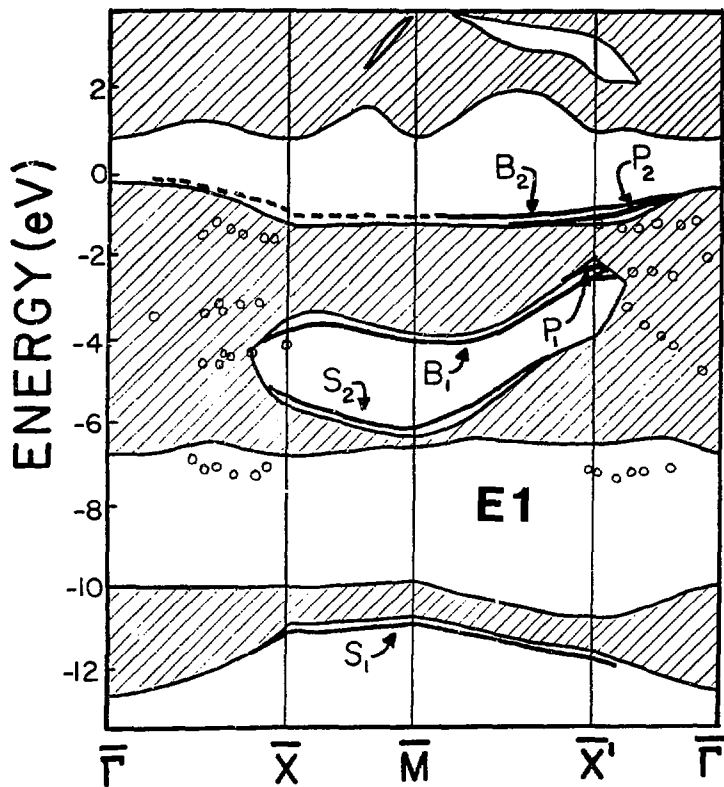


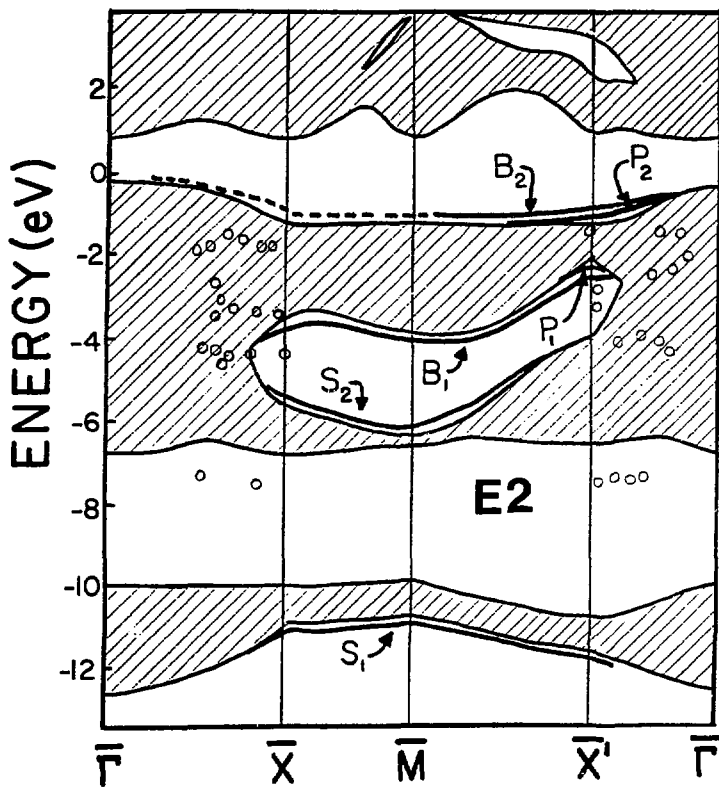
Fig. 6

XBL 792 3213



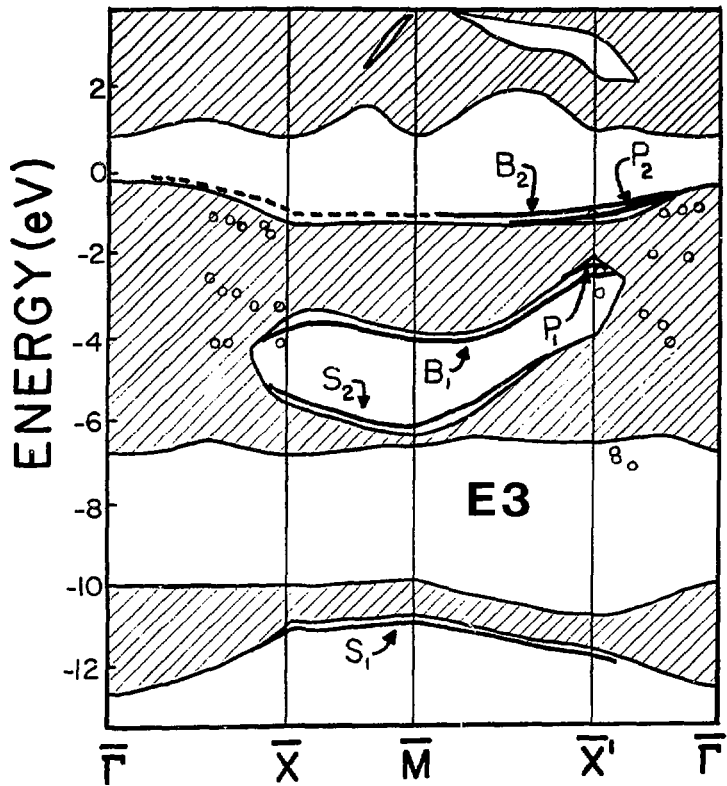
XBL 797-10499

Fig. 7



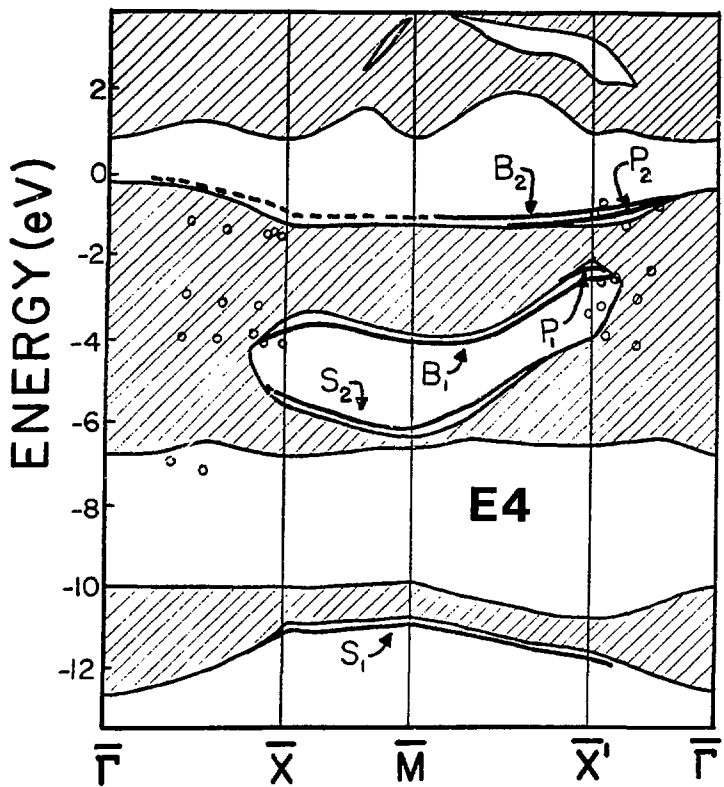
XBL 797-10500

Fig. 8



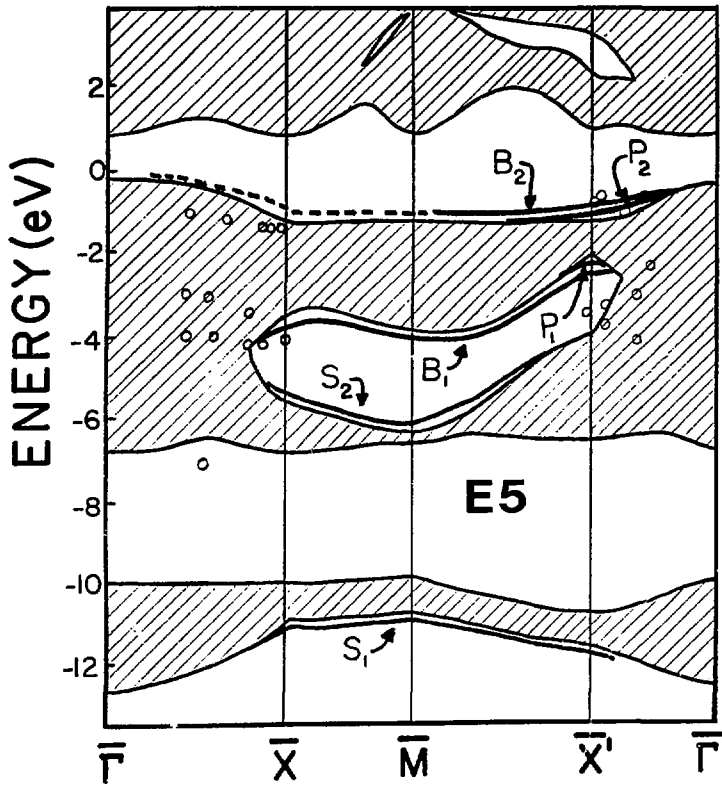
XBL 797-10501

Fig. 9



XBL 797-10498

Fig. 10



XBL 797-10497

Fig. 11

PART II.

CLEAN METAL STUDIES

Here's metal more attractive.

Hamlet, *iii*, 2.

IV. DISPERSION RELATIONS AND RELATED PHENOMENA*
FOR THE (111) FACE OF Au AND Pt

An important question regarding the technique of angle-resolved photoemission (ARP) is the extent to which it can be used to map valence-band dispersion relations. In the case of the 3d and 4d transition metals, studies of copper,¹ nickel,² palladium,³ and silver⁴ show that a model based on the assumption of direct interband transitions may be used, in conjunction with an appropriate choice of final state, to elucidate the valence bands of these materials for several high-symmetry directions in k-space.

It is therefore of considerable interest to extend such studies to 5d metals. The choice of Pt and Au, and the (111) face in particular, was made for several reasons. This face has been studied in greatest detail for the 3d and 4d metals, and is the least difficult to prepare and characterize because it is close-packed and does not tend to reconstruct; in addition, it does not give rise to significant secondary Mahan emission,⁵ which simplifies the analysis. For gold, results using laboratory UV sources are available for comparison,^{5,6} Finally, if one takes into account the difference in Fermi levels and d-bandwidths, the band structures of Pt and Au along (111) are quite similar, which permits a number of useful correlations to be made.

With this background, we have performed normal emission ARP studies of Au(111) and Pt(111) for photon energies of

$6 \leq h\nu \leq 33$ eV. This range of energies enables the determination of the valence-band structure along most of the Λ line, and in particular allows the determination of the d-band energies at Γ . In addition, we have investigated the influence of radiation polarization for Pt(111), and of temperature for Au(111). Final-state effects have also been studied, with particular attention to the choice of the final state, the nature of intensity resonances, and the appearance of a constant-kinetic-energy feature. As will be discussed in detail, all of these effects have their counterparts in the 3d and 4d metals cited above, and all can be understood within the current theoretical framework of ARP.

Section A describes our experimental procedures. In Section B we discuss the dispersion relations obtained, and estimate crystal field parameters. Polarization effects are considered in Section C, and the influence of temperature is elucidated in Section D. Section E is devoted to final-state effects, and the last section provides a summary of our results.

A. Experimental

High-purity crystals of Au and Pt were cut to produce (111) surfaces, and were subsequently polished to 1-micron roughness and etched. The Pt crystal was then installed in a ultrahigh vacuum chamber and cleaned of bulk impurities by a combination of repeated Ar^+ sputtering/annealing cycles

and heating in 10^{-6} torr of O_2 . Cleanliness was monitored by Auger spectroscopy (AES). Both crystals were then mounted for experimentation (orientation to 1° or better as determined by back-reflection Laue photography). Final cleaning just prior to data acquisition was performed in situ by Ar^+ bombardment and annealing at $600^\circ C$ (Au) and $700^\circ C$ (Pt); the Pt sample was characterized by both LEED and AES, and the Au sample by AES.

The photoemission measurements were performed on the 8° branch of Beam Line I at the Stanford Synchrotron Radiation Laboratory. The apparatus used for Au has been described elsewhere,⁷ the only modification being a reduction of the angular acceptance of the CMA to $\pm 2.5^\circ$. The electric field vector of the incident radiation lay in the horizontal plane defined by the Poynting vector of the light and the electron propagation direction; the angle between the latter two was fixed at 63° . In studying Pt(111), a chamber was employed which incorporates a 5.40 mean radius hemispherical analyzer with an angular acceptance of $\pm 3^\circ$, mounted to allow rotation through 2π steradians.⁸ For "s-polarized" spectra, the sample was rotated so that the \vec{E} vector of the light was parallel to the (111) face, the photon propagation direction (\vec{k}_γ) being at 60° relative to the normal. For "p-polarized" light, the \vec{E} vector was effectively rotated 90° from this orientation by moving the sample and analyzer, the angle between \vec{k}_γ and normal again being 60° . The analyzer was then positioned

for detection of electrons propagating normal to the crystal surface. The geometry of each experiment is shown in Figure 1.

Base pressures in both chambers were typically in the 10^{-10} torr range. Samples were oriented in situ using laser collimation, and the normal was determined to 1° or better. The energy resolution (monochromator plus analyzer) varied from ca. 0.1 eV at low-photon energies to ca. 0.2 eV at the high-energy limit. Count rates were excellent, typically on the order of 10^3 to 10^4 sec^{-1} , and a spectrum with adequate statistics could be obtained in 5 to 10 minutes.

Spectra for the entire energy range are shown for Au and Pt (p-polarized radiation) in Figures 2 and 3.

B. Dispersion Relations

Before proceeding with the actual determination of the $E_n(\vec{k})$ relationships, we will discuss the spectra with a view toward identifying the major mechanisms involved.

In accord with previous results,⁵ a surface state peak for Au(111) appears at 0.2 eV binding energy; it rapidly diminishes in intensity with increasing photon energy and by $h\nu = 16$ eV has essentially disappeared. A (111) face surface state has also been observed in Cu and Ag, and general criteria for its existence have been discussed by Heimann et al.⁹ Our binding energy is 0.2 eV less than that reported by Hansson and Flodstrom; this discrepancy will be discussed below.

While density-of-states features do not play a dominant role in the spectra, they may be identified in two cases. For both Pt and Au, a dispersionless shoulder is seen on the leading edge of the d-bands ($E_B \sim 0.3$ eV for Pt, 2.7 eV in Au). No RAPW density of states (TDOS) is available for Pt; for gold, when one includes the difference in energy zero between our measured bands and the theoretical ones, this feature agrees well with the prediction of a TDOS feature at $E_B = 2.4$ eV.¹⁰ This is the only TDOS feature expected; the others would either coalesce under the much stronger direct transitions of similar energy, or be unobservable due to a low cross-section (high s-like initial-state character). This peak grows in relative intensity with increasing photon energy, which results from a decrease of the electronic mean-free path, leading to a breakdown in k-conservation and an enhanced surface DOS contribution. This surface contribution has been studied by Citrin et al. in gold,¹¹ where it was found to be shifted to 0.4 eV lower binding energy relative to the bulk; the growth of this TDOS feature in our spectra would then be consistent with an enhanced surface contribution, the bulk contribution coalescing with the much stronger direct-transition peak. For platinum, the feature at 0.3 eV behaves analogously. A possible origin of this feature is band 6 along the Q line, which is very flat between W and L. Further evidence for the TDOS vs one-dimensional density of states (ODDOS) nature of this peak may be inferred

from its behavior on cooling, as discussed below. Such a shoulder has also been seen in Cu and Ag.^{1,4}

Whenever a flat initial-state band exists, as is the case here for band 2, the possibility of ODDOS features must be considered. While at photon energies of $h\nu \leq 18$ eV a ODDOS peak due to $\Gamma(2,3)$ will not affect our assignment, since it will be clearly separated from the direct transition feature, for higher energies these features can coalesce. As discussed below in the section on temperature dependence, it seems that some of the contribution to the 6.2 eV peak in gold at 18 eV is due to a ODDOS mechanism. This could conceivably cause some error in the experimentally derived location of band 2 near the regions where it begins to disperse, but the error is small and easily correctable if this possibility is kept in mind. In the spectra of the (111) face, in fact, little ODDOS behavior is apparent; for the other low-Miller-index faces, however, the situation is considerably more complicated.⁵

The behavior of the "s-p" plateau was discussed previously,^{1,4} and we comment on it only briefly here. For both Ag and Cu, this feature varied in intensity, reaching a minimum for photon energies corresponding to final states near Γ . Such behavior was observed in this study as well, with the s-p band to d band intensity ratio decreasing by roughly one order of magnitude from $h\nu = 9$ eV (3/4 of the way along Λ to Γ) to $h\nu = 21$ eV (near Γ). We shall return

to this feature in Section D.

A constant kinetic energy feature is also apparent for both crystals, in analogy with results for Ag(111)⁴ and Pd(111).³ For Au, its onset in the spectra is most clearly visible starting for $h\nu = 26$ eV, while in Pt it appears first as a shoulder on the 4.0 eV peak at $h\nu = 23$ eV. Wider energy scans were taken of Pt at photon energies up to 30 eV to confirm the continued presence of the feature, but they are not presented here.

By far the largest portion of the sharp spectral features observed can be assigned to direct transitions. Our spectra agree well with those of Heimann et al. at $h\nu = 16.85$ eV, and Hansson and Flodstrom⁵ for the range $7.0 \leq h\nu \leq 11.6$ eV, with the exception of the location of E_f in the latter. We have assigned these transitions as follows:

1. Relative binding energies were established by spline-fitting the experimental data and visually fitting overlapping peaks as necessary.

2. Band 7 in the theoretical RAPW calculation for gold, which has largely $\vec{G} = [888]$ character (we use the notation of Ref. 10, in which $\Gamma = (000)$, and $L = (444)$) in the middle of the zone, was fitted in this region to the free-electron-like equation $E(k) = \hbar^2 k^2 / 2m^* + V_0$, with the reduced mass m^* and valence-band minimum V_0 as free parameters. This yielded $m^* = 1.17 m_e$ and $V_0 = -3.2$ eV. The fitted final state was then used in the standard way⁴ to obtain initial

state momenta; for this photon energy range, $\vec{k} = [888]$ connects all initial and final states. It was found that such an approach gave somewhat better results than the choice of a true free-electron parabola with V_0 given by $\Gamma(1)$, although the difference was close to the limits of k -resolution in the experiment. For platinum, no theoretical RAPW final-state bands have been reported¹²; accordingly, the fitted Au final state was used, scaled by the ratio of the lattice constants, with the zero of energy shifted to account for the difference in E_F . We feel this procedure is justified given the close similarity of the initial-state theoretical dispersion relations for both materials when this procedure is followed.

3. The Fermi level in Au was taken as the energy at half-height on the onset of the s-p plateau for those photon energies where such an assignment was unambiguous. For $h\nu \leq 16$ eV, however, this onset was masked by the surface state at 0.2 eV; for these spectra, careful monitoring of the analyzer reference voltage enabled assignment of E_F via comparison of these voltages. The work functions so derived showed an RMS scatter of ± 0.05 eV, and our binding energies at $h\nu = 17$ eV agreed with those of Heimann et al.⁶ at 16.85 eV to within 0.07 eV. Accordingly, we feel that the binding energies of Hansson and Flodstrom, which are generally 0.2 eV greater than ours, are too large due to the difficulty in assigning E_F with only low-photon energy data.

In the case of Pt, an analogous approach was employed, except that no surface state was present, while the TDOS feature at 0.3 eV served as its surrogate in masking E_F . At low and high energies, however, this shoulder either vanished or became a well-defined peak; in either case, E_F could then be assigned and analyzer voltages used to set E_f for other energies. With the use of spectra for $h\nu \leq 11$ and $h\nu \leq 28$, the derived work function had an RMS scatter of ± 0.03 eV. The agreement between the s-polarized and p-polarized data was in general excellent (≤ 0.1 eV difference).

As shown in Figures 4 and 5, our data give smooth variations of E with \vec{k} for both crystals, and all the bands are observed in at least part of the zone. The band energies are tabulated in Table I for selected values of \vec{k} ; our data may be recovered from Figures 4 and 5 by using k^2 and E_B to back-calculate $h\nu$, with $E(k) = h\nu - E_B$. The assignment of the band 1 transitions in Pt, which are admittedly weak in these spectra, was aided by additional data from higher ($h\nu > 40$ eV) energy spectra¹³; all other transitions, however, were easily assigned with the lower-energy data. For simplicity, we have not included on this plot either the surface-state or indirect-transition peaks described earlier. Band 4 in Pt cannot be assigned for p-polarization radiation near Γ because the spectra are dominated by the band 2,3 and 5,6 features for these photon energies, but an assignment can be made from s-polarized light spectra and will be

presented below. It appears that there is a need to adjust the theoretical energy zero in gold by approximately 0.2 eV down to fit our results. This discrepancy is attributable to the use of the 4.2°K lattice constant in the original RAPW calculation. Subsequent work¹⁴ using the 300°K value has shown a shift "of the majority of the bands" by ca. 0.2 eV down. This is consistent with our observations; further, in the case of Pt, where the RAPW calculation is for a 300°K crystal, no shift is suggested by our data. From the band energies at Γ , given in Table I, it follows that the ($\Gamma_8 - \Gamma_8$) splitting in both Pt and Au is virtually identical to theory, while Γ_7 is too close to the upper Γ_8 level by about 0.15 eV in both cases. Most likely, these discrepancies in the theory are due to difficulties in calculating the spin-orbit interaction, and in determining E_p .

By far the most dramatic difference between theory and experiment occurs in the actual shape of the bands mapped. For both crystals, bands 5,6 have a larger splitting than predicted, and for \vec{k} nearer to Γ than expected. Also, bands 3,4 do not repel near (5,5,5) as much as the theory would suggest. That this behavior occurs in both crystals gives us confidence in its certitude, and precludes its being due to an artifact of our analysis, such as a poor choice of final state. It is important to note that these features are insensitive to the exact nature of the final state; while a variation in the final state used will alter the region

of the zone in which the effects occur, it cannot alter the relative splittings or absolute energies of the peaks, and the discrepancies will remain. In addition, our quasi-free-electron final state fits the RAPW conduction band quite well midway along Λ , where much of the discrepancy is observed. This behavior is not observed in Ag(111), but in Pd(111)³ the (5,6) splitting is characteristically 0.2 eV larger than predicted; band 3(Λ_3) is not obtained for this crystal along all of the Λ line, but the results presented strongly suggest that band 4(Λ_1) also extends to significantly lower binding energies midway along Λ than is theoretically predicted. It is interesting to note that the relativistic KKR calculation of Sommers and Amar¹⁵ for Au shows some qualitative similarity with the band 3-band 4 narrowing observed near (5,5,5), and the larger band 5-band 6 splitting observed; however, their d-band width is much too large due to the use of 2/3 Slater exchange, and XPS measurements¹⁶ have shown the work of Christensen and Seraphim to give much better agreement with the photoemission density of states.

From the band energies at Γ , we may also derive crystal field parameters, as discussed in our Ag(111)⁴ paper. These results are presented in Table II. For Pt(111), the band energies at Γ were assigned using the data for s-polarized radiation, which enabled the assignment of band 4 up to 24 eV, corresponding to an initial state wavevector of magnitude $|k|^2 \sim 187$ for this binding energy. The comparison of ξ_{5d}

with that obtained in atomic structure calculations¹⁷ is excellent for both Pt and Au, within roughly 4% of the predicted value. This agreement is in part fortuitous, as ξ will be different in the solid state, and in fact may be expected to depend on the binding energy of the associated band as well. As discussed in Anderson's theoretical paper on Pt,¹² ξ is expected to vary from ca. 0.54 eV to 0.76 eV; using the theoretical energies at Γ , however, gives results that are significantly different from those obtained experimentally, and actually produces a value of ξ_{5d} for Pt that is greater than that for Au, in qualitative as well as quantitative disagreement with the atomic values. These considerations suggest that the presently available theoretical calculations are not incorporating the spin-orbit interaction in a satisfactory manner, or that the crystal potential used is sufficiently in error to produce these discrepancies.

It is interesting to compare values of $10Dq$ for the group VIII and IB transition metals. Using our results in combination with values of critical points reported in the ARP literature, we have compiled $10Dq$ values for Ni, Cu, Pd, Ag, Pt, and Au (Table III). The empirical Ni value is anomalous, and may be due to an improper assignment of Γ_{25} . Overall, however, the trends are obvious and consistent with expectation: $10Dq$ increases as one proceeds either to the left, or down, in the periodic table.

C. Polarization Effects

In materials such as copper, where relativistic effects are small and the eigenfunctions therefore transform as the single space group of the crystal, it is well-known that an appropriate choice of experimental geometry can allow the observation of initial states of particular symmetry, as determined by the requisite selection rules.¹⁸ Such is also the case for Pt(111), although the situation is more complicated due to spin-orbit coupling, which gives eigenfunctions transforming as the associated double group.

Our results for s- and p-polarized radiation are shown in Figure 6. Let us note first of all that for the "p-polarized" case, the polarization vector $\vec{\eta}$ is in fact a mixture of the two components ($\hat{\eta}_1 \perp [111]$ and $\hat{\eta}_2 \parallel [111]$) with about 60% η_2 character. In addition, the finite angular resolution of the spectrometer will break the selection rules, which can be rigorously derived only for mirror-plane emission. As a consequence, only diminution and not disappearance of peaks can be expected, and this is in fact observed.

The major changes in the spectra are as follows. First, it is seen that the band (5,6) doublet shows much larger intensity variations for s-polarized ($\hat{\eta} \sim \hat{\eta}_1$) radiation, with the 5 to 6 ratio being smaller for the s case. Analogously, for photon energies (s-polarization) where bands 2 and 3 are nearly degenerate ($h\nu \approx 18$ eV), this feature is seen to be weaker in comparison to bands 5 and 6; such

behavior is least ambiguous for $h\nu \geq 22$ eV. From the spectra at 15 to 17 eV, the band 4 peak is seen to be larger in comparison to that of band 5 for s-polarized light. Finally, there is the seeming absence of the band 3 peak for s-polarization, $h\nu = 13$ to 15 eV. Taken together, these results lead to the conclusion that bands 3 and 5 are suppressed for s-polarization relative to bands 2, 4, and 6, or the alternate interpretation, that bands 2, 4, and 6 are suppressed for p-polarized light.

To distinguish between these possibilities, we must turn to group theory. The general selection rule for transitions is of course well-known¹⁹: For initial and final states transforming as Γ_i and Γ_f , and a transition operator as Γ_γ , the direct product $\Gamma_f^* \times \Gamma_\gamma \times \Gamma_i$ must contain the identity representation if a transition is to occur. Equivalently, the transition vanishes unless Γ_f is found in $\Gamma_\gamma \times \Gamma_i$, or Γ_γ in $\Gamma_f \times \Gamma_i$.

The initial-state symmetries will be Λ_4 , Λ_5 , or Λ_6 , by analogy to gold.¹⁰ The transition operator is $\vec{A} \cdot \vec{p}$, which reduces to $\vec{\eta} \cdot \vec{r}$; analogous to the nonrelativistic case, this transforms as a vector and we have

$$\begin{aligned} \vec{\eta} \parallel [111], \vec{\eta} \cdot \vec{r} \sim z, \Lambda_1 & \quad \text{"p-polarized"} \\ \vec{\eta} \perp [111], \vec{\eta} \cdot \vec{r} \sim (x, y), \Lambda_3 & \quad \text{"s-polarized"} \end{aligned}$$

From the character tables of Elliot²⁰ and Dresselhaus²¹ for the double group,

$$\Lambda_1 \times \Lambda_i = \Lambda_i$$

and

$$\Lambda_3 \times \Lambda_i = \Lambda_3, \quad i = 1, 2$$

$$\Lambda_6, \quad i = 4, 5$$

$$\Lambda_{1+2+3}, \quad i = 3$$

$$\Lambda_{4+5+6}, \quad i = 6$$

The final state is $\Lambda_1 \times D^{1/2} = \Lambda_6$, since it must be symmetric in the limit of reaching the detector.¹⁸ Then we have the selection rules

$$\text{s-polarized} \quad \Lambda_i = \Lambda_4, \Lambda_5, \Lambda_6$$

$$\text{p-polarized} \quad \Lambda_i = \Lambda_6$$

These selection rules are consistent with our data if we take the spectral intensities as evidence of suppression of bands 2, 4, and 6 for p-polarization, and assign the symmetries

$$\Lambda_6 \quad - \text{bands } 3, 5, 7$$

$$\Lambda_{4+5} \quad - \text{bands } 2, 4, 6$$

The calculation of Anderson¹² for Pt does not provide the symmetries of the Λ bands. If we refer to the calculation of Christensen and Seraphim¹⁰ for Au, which should also apply to Pt, we see that these empirical assignments are inconsistent with those given theoretically. In that calculation, however, band 7 is assigned as Λ_4 , which in our notation is unreasonable, since the Λ_4 representation is not symmetric under the elements \bar{E} , $2C_3$, σ_V , and $\bar{\sigma}_V$ of the

double group; it thus appears that the double group notation of Ref. 10 is different from that of Dresselhaus. The Au band structure of Sommers and Amar,¹⁵ which specifically uses the notation of Elliot, gives initial state assignments different from those of Christensen and Seraphim, and more consistent with those presented here. As noted previously, however, there are several artifacts in that work, such as overlarge d-band width, inaccurate TDOS, and spurious band-crossings, which limits its usefulness. Accordingly, neither theoretical assignment is found to be consonant with that determined experimentally.

D. Thermal Behaviour

That ARP spectra can undergo dramatic changes with variation of temperature has been well-established in the case of Cu(110).²² In general, such changes will result from an enhancement of indirect transitions with increasing temperature; this is due to an increase in the number of populated phonon modes and concomitant increase in the number of channels available for phonon-assisted indirect transitions. Correspondingly, cooling of a sample may be expected to enhance the contribution of direct transitions, and for a material such as gold, which has a comparatively low Debye temperature and hence higher susceptibility to indirect processes, one may expect particularly significant changes.

We show in Figures 7 and 8 spectra for Au(111) at room temperature (ca. 300°K) and cooled to approximately 150°K. It is apparent that the most dramatic changes occur for low photon energies (Figure 7), where the reduction in temperature leads to a marked enhancement of the spectral features over background. There are two mechanisms that could account for this enhanced contrast: reduction of the inelastic background,²³ or enhancement of direct transitions due to a diminution in phonon-assisted indirect transitions.²⁴ As we shall now discuss, there are features in our spectra which indicate that both mechanisms may be involved.

The primary indication of a reduction in phonon-assisted processes may be taken from the photon energy dependence of the spectra. As the probability for phonon-induced indirect transitions increases with decreasing phonon wavevector,²⁴ we may think of such processes in first order (i.e., when they contribute only weakly to the spectrum) as producing a net broadening in the initial-state wavevector, or "thermal broadening." The band width ΔE of a feature will depend not only on this Δk but on the region of the zone in which the transition originates. In particular, it will be for those transitions originating at points where the bands are steep that ΔE will most strongly depend on Δk ; this is where the largest change upon cooling is expected. Conversely, smaller changes should be apparent on cooling for regions of the zone where the bands are flat. As seen in Figure 4,

it is thus for low photon energies that we expect cooling to have its greatest effect, while by $h\nu = 20$ eV, as the initial states approach Γ , the spectra should be less affected. That this is precisely the behavior observed in Figures 7 and 8 indicates that a reduction in thermal broadening may be at least partially responsible for the enhancement observed.

There are several other features in these spectra which may be used in attempting to obtain a more complete explanation. We first note the behavior of the surface state intensity at low photon energies; it is clear that this transition is enhanced at low temperatures. Since this feature is dispersionless for normal emission, our discussion above would indicate it to be relatively insensitive to temperature changes. On the other hand, the processes involved in determining the intensity of surface states are poorly understood, and it is quite possible that a competing mechanism, for example surface-phonon-induced indirect transitions, could be the cause of this change. In fact, results of analogous experiments for Ag(111) show a similar enhancement of the surface state,²⁵ without any other significant changes in the spectral appearance. As silver has a higher Debye temperature than gold, this would tend to indicate that phonon-assisted indirect transitions, which contribute both to the inelastic tail and k-broadening, are less important in Ag, and correspondingly that the mechanism governing surface state intensity losses is less dependent on the bulk properties

of the material involved. This propensity for indirect transitions in Au vis-a-vis Ag is also observed for the other low-Miller-index faces.²⁶

The other major feature that provides insight is the intensity of the s-p plateau. We have calculated the ratio of the s-p to d-band intensities, subtracting the apparent background, for both sets of data. As seen in Table IV, these values are virtually identical for both temperatures. The implications of this are twofold. The first is that the mechanism that produces the s-p plateau cannot be that of phonon-induced indirect scattering since this would necessarily lead to a decrease of the s-p to d-band ratio with cooling. It thus appears most likely that the s-p plateau arises from some process analogous to that producing TDOS features, which would be relatively insensitive to changes in temperature. In fact, our spectra contain features that demonstrate this difference in temperature dependence between ODDOS and TDOS processes. As mentioned earlier, the shoulder at the leading edge of the d-bands may be assigned as a TDOS feature; it is seen to be insensitive to cooling. On the other hand, for a ODDOS feature such as that observed as a component of the peak at 6.2 eV, $h\nu = 18$, which arises due to the flatness of bands (2,3) near Γ , cooling produces a significant diminution of intensity.

The second implication of the thermal independence of the s-p to d ratio is that thermal broadening cannot be the

whole story in explaining the spectral enhancement at low temperatures. If such were the case, the ratio would of necessity drop at low temperatures, due to the enhancement of the d intensity. On the other hand, any mechanism leading to a reduction in the background would leave the ratio unaltered, since the background is subtracted when obtaining this parameter. This strongly suggests that phonon contributions to the inelastic tail must play a strong, and perhaps dominant, role in determining the spectral contrast.

E. Final-State Dependent Features

While the analysis of our data has to this point concentrated on initial-state features, there are also features in the spectra which give insight into final-state effects. We have already discussed our use of a free-electron-like state for band mapping, and while such a method is quite adequate away from the center or edges of the zone, it becomes suspect where the conduction bands are expected to undergo significant perturbation. Figure 9 shows the theoretical initial- and final-state band structure for Au(111), along with our modified plane-wave final state. As can be seen, band 7 near Γ becomes quite flat, and in fact a gap may be expected between it and the next band, which will have a significant amount of $\vec{G} = [888]$ character. In this region, the exact nature of the final state becomes much less clear. We have accordingly taken spectra for both Pt and Au with a finer

energy mesh in the photon energy range where this part of band 7 is expected to be accessed. As shown in Figures 10 and 11, dramatic intensity resonances occur as the final state approaches Γ . There are two possible explanations for this, the first being associated with the change in dispersion of band 7 near Γ , due to increased f character, and the second with the presence of the gap.

Of these two explanations, only the former is consistent with these data and the results of studies for other faces. Such resonances have already been reported in Ag(111)⁴ and Pd(111).³ Work in our laboratory has also shown their presence in Ag(110) and Ag(100).²⁷ In all these cases, the RAPW final-state band is quite flat near Γ . For Au(100), however, and by extension for Pt(100), the final-state band near Γ is not flat but rather peaks near $\vec{k}_1 = (0, 2, 0)$ and drops as it approaches Γ . Our studies on Pt(100)²⁹ show that, unlike for Pt(111), the intensity resonances are quite weak. Were these resonances associated with the gap, such would not be the case.

To more fully examine this behavior, we have calculated normalized intensities for the $\Lambda(2,3) \rightarrow \Lambda(7)$, $\Lambda(4) \rightarrow \Lambda(7)$, and $\Lambda(5,6) \rightarrow \Lambda(7)$ transitions in Au(111) and Pt(111) as a function of photon energy. These are shown in Figures 12 and 13. In both cases, peak areas were corrected for total photon flux and data accumulation time; in the case of Pt, the analyzer transmission function was also known and used.

Unfortunately, recent indications are that the photon density may undergo changes of unknown magnitude with energy on the 8° line, so that our results could contain an associated error. Such a correction would be expected to be monotonic, however, and hence would alter only the shape and not the existence or location of the resonances. While these results cannot be presumed quantitatively definitive, therefore, they should be qualitatively correct.

As the figures show, all three transitions undergo resonances in intensity with photon energy, with the $A(5,6)$ - $A(7)$ resonance being the least intense. In the case of Pt, the resonance is consistent for all three transitions, and yields an energy of $E_7(\Gamma) = +16.6$ eV relative to E_p . For gold, the $A(5,6)$ transition is ca. 1 eV too low, and using the remaining two values yields $E_7(\Gamma) = +16.4$ eV. This latter value compares not unfavorably with the theoretical value of 15.6 eV.³⁰ It is also interesting to note, especially for Pt, the asymmetry of the resonance, with the line edge being sharper on the gap side. This is a pleasing result; as itinerant final states are rigorously forbidden in the gap in the limit of an infinite solid, one would expect an effect due to bulk bands to disappear more rapidly in the gap. In other words, the width of the final state may be expected to be asymmetric, with a smaller value on the gap side. Unfortunately, a monochromator-derived function could also produce such an asymmetry, and elucidation of this effect

must await more definitive experiments.³¹

The other final-state effect of interest is a constant kinetic energy feature, in both Au and Pt, satisfying the equation $E_B \approx hv - 16$. Analogous behavior was observed in Ag(111),⁴ and was attributed to scattering and subsequent ejection of electrons of higher kinetic energy into the very high density of states region at 16 eV above E_F , composed of bands 7 and 8. We note that as hv decreases, this feature should proceed to lower apparent binding energy, merging with the band (2,3) resonance; this is clearly observed in both crystals. It is interesting that this feature appears stronger here than in Ag; comparison of the RAPW calculations for Ag and Au shows that both bands 7 and 8 are flatter near Γ in Au, which accounts for the intensity difference and lends further credence to the mechanism proposed.

We have also studied the behavior of this feature in Pt(111) for off-normal emission. As seen in Figure 14, the peak is most intense at normal, and falls off symmetrically about the (111) axis, having disappeared by a 15° takeoff angle. This would lead one to suspect that it is the flatness of band 8, which is unique to the Λ direction, and not just that of band 7 near Γ , which provides the high conduction band density-of-states necessary for this process. In fact, in Ag(100)²⁷ and Pt(100)²⁹ no such constant kinetic energy feature is observed, although resonances in direct transition intensities, analogous to those reported in Ag(111), are

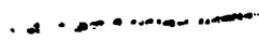
observed. Taken together, these observations strongly indicate a mechanism that involves scattering into the $\Lambda(8)$ band, followed by crossing to $\Lambda(7)$ and subsequent emission from the crystal.

F. Summary

We have presented results of normal emission ARP studies for variable photon energy. Specifically, we have mapped bands along most of the Λ line for Pt and Au. Comparison of these results to theory shows that, unlike for simpler cases, the predicted band structures do not agree within experimental error with the empirically derived dispersion relations. Several other aspects of the spectra have been noted and discussed, including a surface state, constant kinetic-energy feature, and density-of-states features. By investigating the effect of cooling for Au(111), we have been able to gain some insight into the mechanisms giving rise to the "s-p plateau" and determining the spectral contrast, as well as distinguishing one- and three-dimensional density-of-states features. Through the use of polarization selection rules and our observed spectral intensities, we have determined the initial state symmetries for Pt(111). We have also investigated resonances in the transition probabilities due to final-state effects.

It is clear that this work, in combination with that cited for Cu, Pd, Ni, and Ag, shows that the use of ARP data,

in conjunction with the direct-transition model and an appropriate final state, provides a method of general utility for mapping bands in (111) single crystals. The logical extension of such studies is to other low-Miller-index crystal faces, and such work is presently underway. Other avenues of investigation that this work opens are the use of polarization effects to assign initial-state symmetries for relativistic band structures, and the elucidation and characterization of final-state resonances. The latter subject, in particular, is of considerable interest, as it should shed light on the exact nature of the final state near--and in--gaps predicted for the infinite solid limit.



REFERENCES

* Work performed in collaboration with R.F. Davis, S.D. Kevan, G. Thornton, and D.A. Shirley

- 1) J. Stöhr, P.S. Wehner, R.S. Williams, G. Apai, and D.A. Shirley, Phys. Rev. B17, 587 (1978); J.A. Knapp, F.J. Himpsel, and D.E. Eastman, Phys. Rev. B19, 4952 (1979); P. Thiry, D. Chandrossis, J. Locante, C. Guillot, R. Pinchaux, and V. Petroff, Phys. Rev. Lett 43, 32 (1979).
- 2) D.E. Eastman, F.J. Himpsel, and J.A. Knapp, Phys. Rev. Lett. 40, 1514 (1978); F.J. Himpsel, J.A. Knapp, and D.E. Eastman, Phys. Rev. B19, 2919 (1979).
- 3) F.J. Himpsel and D.E. Eastman, Phys. Rev. B18, 5236 (1978).
- 4) P.S. Wehner, R.S. Williams, S.D. Kevan, D. Denley, and D.A. Shirley, Phys. Rev. B19, xxxx, and references therein.
- 5) G.V. Hansson and S.A. Flodstrom, Phys. Rev. B18, 1572 (1978).
- 6) P. Heimann, H. Miosga, and H. Neddermeyer, to be published, 1.
- 7) J. Stöhr, G. Apai, P.S. Wehner, F.R. McFeely, R.S. Williams, and D.A. Shirley, Phys. Rev. B14, 5144 (1976); P.S. Wehner, PhD Thesis, Univ. of Calif., Berkeley, April 1978 (LBL-7622).
- 8) A more complete description will be published in the near future.
- 9) P. Heimann, H. Miosga, and H. Neddermeyer, to be published, 2.

- 10) N.E. Christensen and B.O. Seraphim, Phys. Rev. B4, 3321 (1979).
- 11) P.H. Citrin, G.K. Wertheim, and Y. Baer, Phys. Rev. Lett. 41, 1425 (1978).
- 12) O.K. Anderson, Phys. Rev. B2, 883 (1970).
- 13) S.D. Kevan, K.A. Mills, R.S. Williams, and D.A. Shirley, unpublished data.
- 14) N.E. Christensen, Phys. Rev. B13, 2698 (1976).
- 15) C.B. Sommers and H. Amar, Phys. Rev. 188, 1117 (1969).
- 16) D.A. Shirley, Phys. Rev. B5, 4709 (1972).
- 17) F. Hermann and S. Skillman, Atomic Structure Calculations (Prentice Hall, Englewood Cliffs, New Jersey 1963).
- 18) J. Hermanson, J. Jerson, and G. Lapeyre, Phys. Rev. B12, 5410 (1975).
- 19) M. Tinkham, Group Theory and Quantum Mechanics (McGraw Hill, New York, 1974).
- 20) R.J. Elliot, Phys. Rev. 96, 280 (1954).
- 21) G. Dresselhaus, Phys. Rev. 100, 580 (1955).
- 22) R.S. Williams, P.S. Wehner, J. Stöhr, and D.A. Shirley, Phys. Rev. Lett. 39, 302 (1977).
- 23) J.M. Ballantyne, Phys. Rev. B6, 1436 (1972); B.L. Henke, J. Liesegang, and S.D. Smith, Phys. Rev. B19, 3004 (1979).
- 24) N.J. Shevchek, J. Phys. C, L555 (1977) and Phys. Rev. B16, 3428 (1977).

- 25) D.R. Denley, PhD Thesis, Univ. of Calif., Berkeley, July 1978 (LBL-9482). We note that the possibility of surface reconstruction with cooling cannot be entirely ruled out; it is, however, highly unlikely for the (111) face. In addition, studies have shown the surface state to be most intense for this face (Ref. 9), so that reconstruction would be expected to lead to diminution, not enhancement.
- 26) G.V. Hansson and S.A. Flodstrom, Phys. Rev. B17, 473 (1978), and Ref. 5.
- 27) K.A. Mills, R.F. Davis, R. Watson, G. Thornton, and D.A. Shirley, to be published.
- 28) N.E. Christensen, Phys. Stat. Sol. B 51, 551 (1972), and Ref. 10.
- 29) G. Thornton, R.F. Davis, K.A. Mills, and D.A. Shirley, to be published.
- 30) J. Hermanson, J. Anderson, and G. Lapeyre, Phys. Rev. B12, 5410 (1975), have studied this effect using angle-integrated CIS spectroscopy and report $15 \text{ eV} \leq E_7(\Gamma) \leq 16 \text{ eV}$. Their experiment, however included the $\Lambda(5,6) \rightarrow \Lambda(7)$ transition, which we see here to give a characteristically low value for $E_7(\Gamma)$.
- 31) A recent investigation of Cu(110) [E. Dietz and F.J. Himpsel, Solid State Comm. 30, 235 (1979)] has shown the presence of similar final-state resonances in this material. They have interpreted their results in terms

of a cessation of dispersion for band gap photoemission; our work on Ag(110) (Ref. 27) does not agree with this interpretation, and discusses the question of gap photoemission in detail. For the study conducted here, the flatness of the valence bands near Γ , where the only gap is expected, renders this question unimportant.

- 32) N.E. Christensen, Phys. Rev. B14, 3446 (1976).
- 33) N.E. Christensen, Phys. Stat. Sol. B 54, 551 (1972).
- 34) G.A. Burdick, Phys. Rev. 129, 138 (1963).
- 35) C.S. Wang and J. Calloway, Phys. Rev. B15, 298 (1977).

Table I
 Values of Valence Bands Along Λ in Platinum and Gold (eV)

k (units of Ref. 10)		Energy (eV)					
		Band 1	Band 2	Band 3	Band 4	Band 5	Band 6
000 (Γ)	Au	-	5.90	5.90	4.45	3.55	3.55
	Pt	-	4.07	4.07	2.80	1.40	1.40
111	Au	-	5.90	5.90	4.45	3.95	3.48
	Pt	-	4.15	3.98	2.78	1.75	1.16
222	Au	-	6.15	5.65	4.55	3.60	2.90
	Pt	-	4.05	3.65	3.00	1.10	0.55
333	Au	6.85	6.30	4.95	3.90	2.85	2.50
	Pt	5.65	-	-	2.05	0.40	-
Λ_{\min}^a	Au	7.10 (2.40)	6.45 (2.75)	5.90 (0.00)	4.65 (2.50)	3.95 (1.15)	3.55 (0.00)
	Pt	6.10 (2.30)	4.07 (0.00)	4.07 (0.00)	3.05 (2.10)	- (0.95)	1.40 (0.00)

^aValue in parenthesis is k_x corresponding to the binding energy at which the band is most tightly bound.

Table I
Derived Crystal Field Parameters

Source	Parameter	Crystal	
		Au	Pt
Experimental fit (eV)	ξ_{5d}	.71 ± .05	.66 ± .05
	10Dq	1.22 ± .05	1.78 ± .05
Force fit (eV) ^a	ξ_{5d}	.74	.63
	10Dq	1.28	1.70
Theoretical fit (eV) ^b	ξ_{5d}	.56	.59
	10Dq	1.36	1.93

^a Using the value of ξ_{5d} from atomic structure calculations (Ref. 11).

^b Using splittings at Γ from RAPW calculations (Refs. 10,12).

Table III
Values of $10Dq$ for Various Transition Metals

		Ni	Cu	Pd	Ag	Pt	Au
10Dq	Expt.	0.7 ^b	0.73	1.40 ^c	.865	1.78	1.22
	Thy.	1.13	0.8	1.44	.880	1.93	1.36
Ref.	Expt.	2	1	3	4	a	a
	Thy.	35	34	32	28	12	10

^aThis work.

^bThis value may be anomalous as discussed in the text.

^cValue ignoring spin-orbit splitting (i.e., $\Gamma_{12} - \Gamma_{25'}$).

Table IV
Ratio of s-p Intensity to d-Band Intensity
at 300° and 150°K

Photon energy	Intensity ratio ^a	
	300°	150°
9	.37	.46
12	.11	.12
15	.08	.07
18	.05	.06
21	.03	.04

^aEstimated uncertainty is 20%.

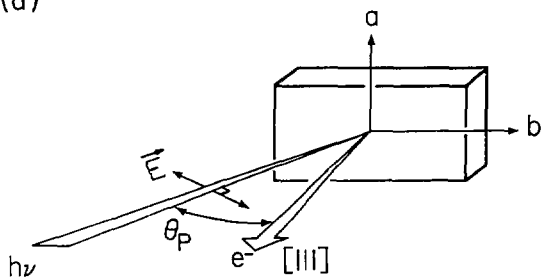
FIGURE CAPTIONS

- Figure 1. Experimental geometries employed: (a) "p-polarized" radiation. For gold, $a = [\bar{1}\bar{1}2]$, $b = [\bar{1}10]$, $\theta_p = 62.7^\circ$. For Pt, $a = [\bar{1}10]$, $b = [11\bar{2}]$, $\theta_p = 60^\circ$. (b) "s-polarized" radiation.
- Figure 2. Selected photoemission spectra at normal emission for Au(111) in the energy range $6 \leq h\nu \leq 33$ eV.
- Figure 3. Selected spectra, normal emission and p-polarized radiation, for Pt(111) in the energy range $8 \leq h\nu \leq 33$ eV.
- Figure 4. Empirical (circles) and theoretical (solid lines, Ref. 10) valence-band dispersion relations in Au(111). A partial photon energy scale is indicated along the top.
- Figure 5. Empirical (circles) and theoretical (Ref. 12) valence bands for Pt(111).
- Figure 6. Comparison of spectra for Pt(111) using s- and p-polarized light, for selected photon energies.
- Figure 7. Spectra at 300°K and 150°K of Au(111), in the low photon energy region.
- Figure 8. Au(111) spectra for higher photon energies at 300°K and 150°K .

- Figure 9. Theoretical band structure (solid lines, Ref.10) and the fitted quasi-plane-wave final state used here (solid circles) for Au along the Λ line. Bands are numbered sequentially starting at the lowest energy.
- Figure 10. Selected spectra with a finer photon energy mesh for Au(111). Note particularly the resonances in intensity of the main features as $h\nu$ changes.
- Figure 11. Spectra of Pt(111) using a smaller energy step. The band (2,3) and (4) resonances may be followed in this figure.
- Figure 12. Plot of intensities of the band (2,3) (4), and (5,6) peaks for Pt(111) as a function of photon energy. Approximate maxima are indicated; the ordinate is the relative intensity for a given peak, normalized to its maximal value.
- Figure 13. Normalized intensities for the (2,3), (4), and (5,6) peaks in Au(111) as a function of photon energy.
- Figure 14. Spectra of Pt(111), p-polarized radiation at 26 eV, for various electron takeoff angles relative to the surface normal. In the geometry of Figure 1a, the angle θ_e corresponds to

takeoff directions in the plane defined by the $[111]$ and $[11\bar{2}]$ directions, with θ_e being negative for rotations towards $[11\bar{2}]$; θ_e corresponds to directions in the $[\bar{1}10] - [111]$ plane, being negative for rotations towards $[\bar{1}10]$. (a) polar dependence, $\theta_e = 0$. θ_p is fixed at 60° . (b) azimuthal dependence, $\theta_e = 0$. θ_p is fixed at 60° . The dashed line is for $E_k = 16$ eV.

(a)



(b)

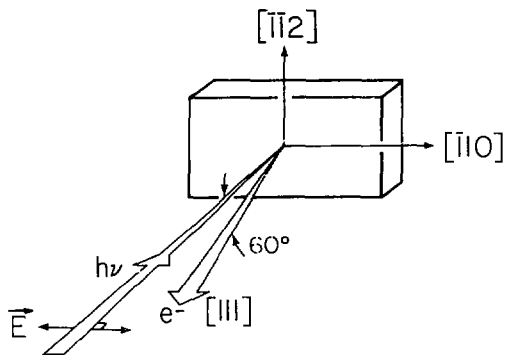


Fig. 1

XBL 797-2119

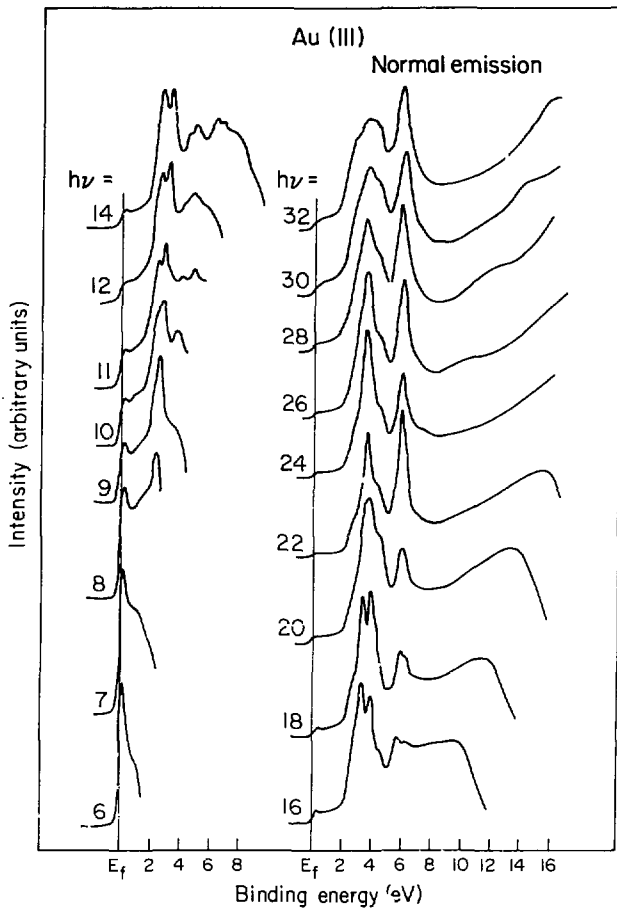


Fig. 2

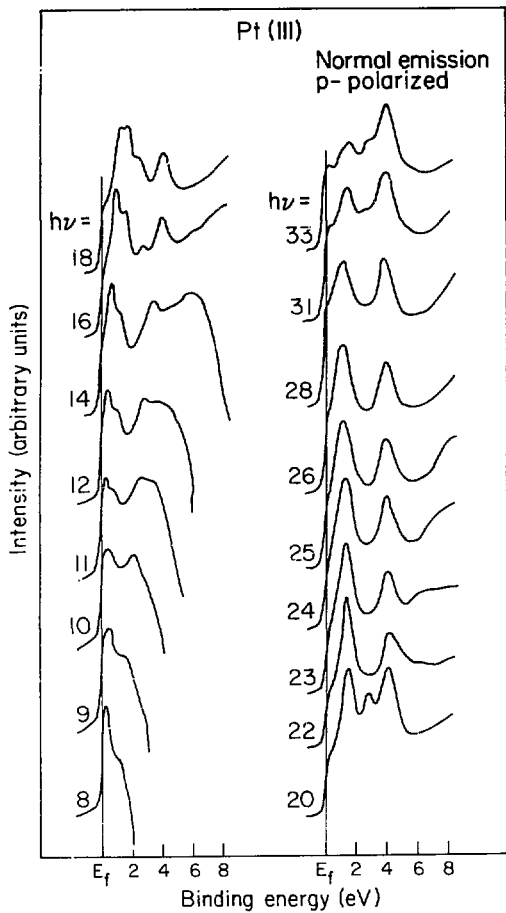


Fig. 3

XBL 797-2112

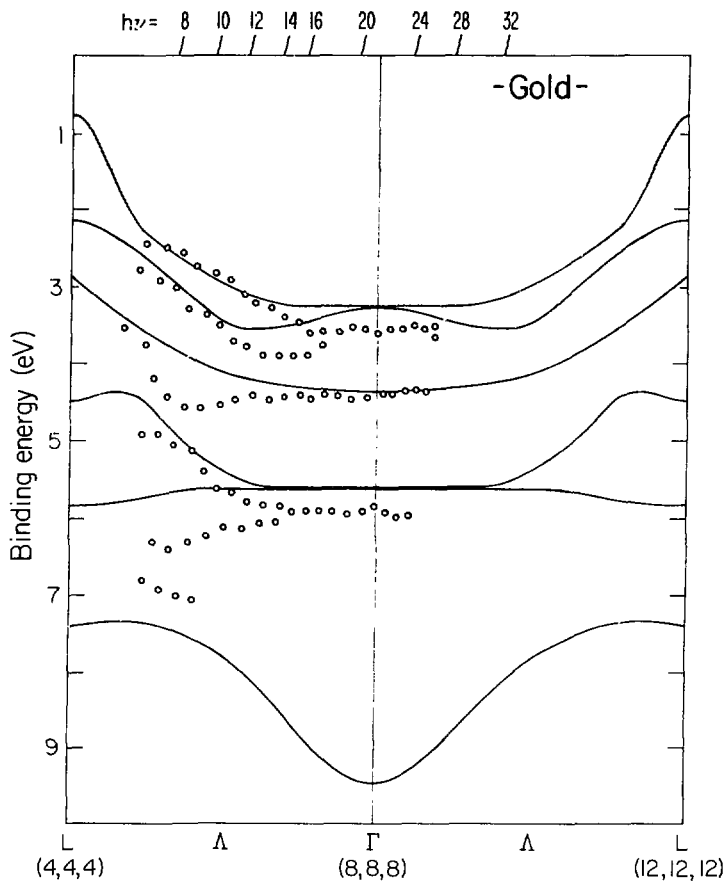


Fig. 4

XBL 797-2117

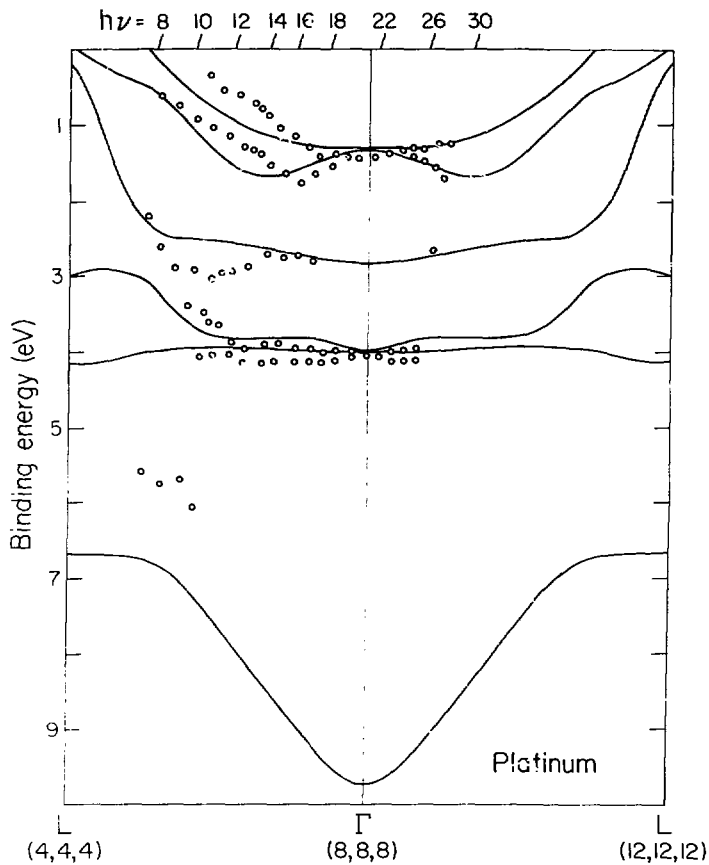


Fig. 5

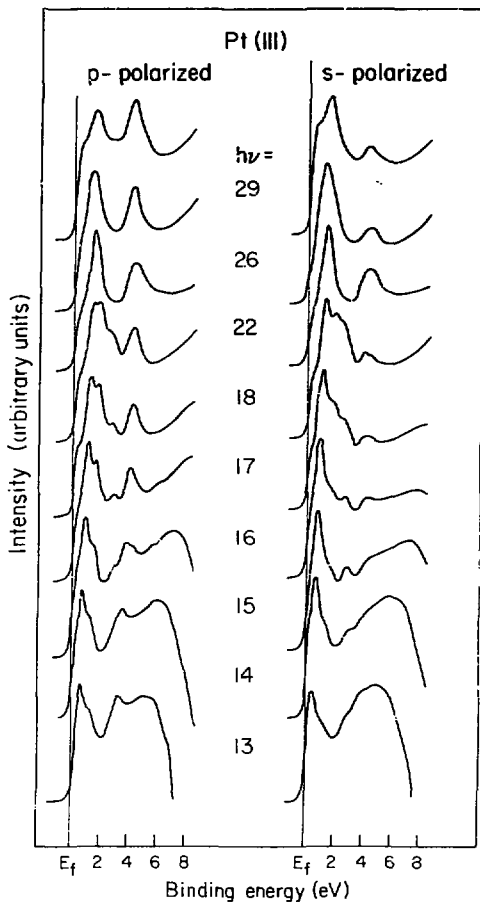


Fig. 6

XBL 797-2108

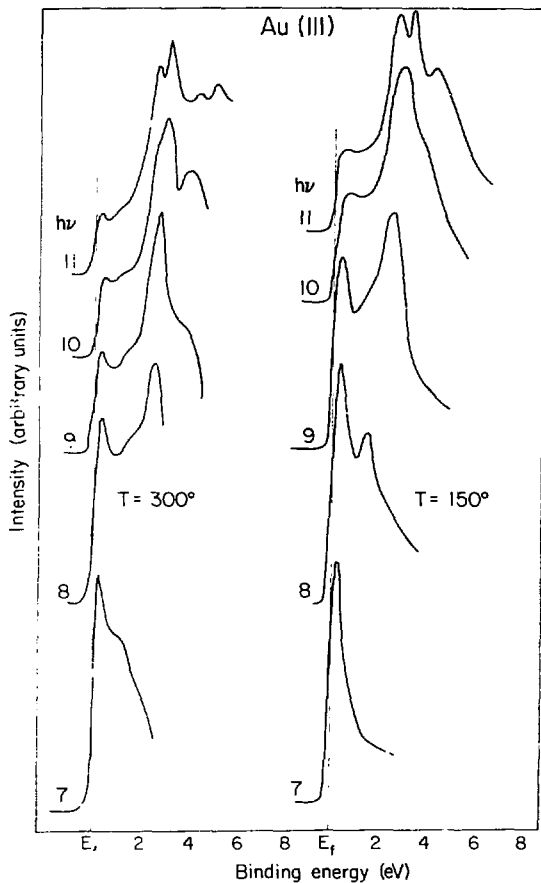


Fig. 7

XBL 797-2107

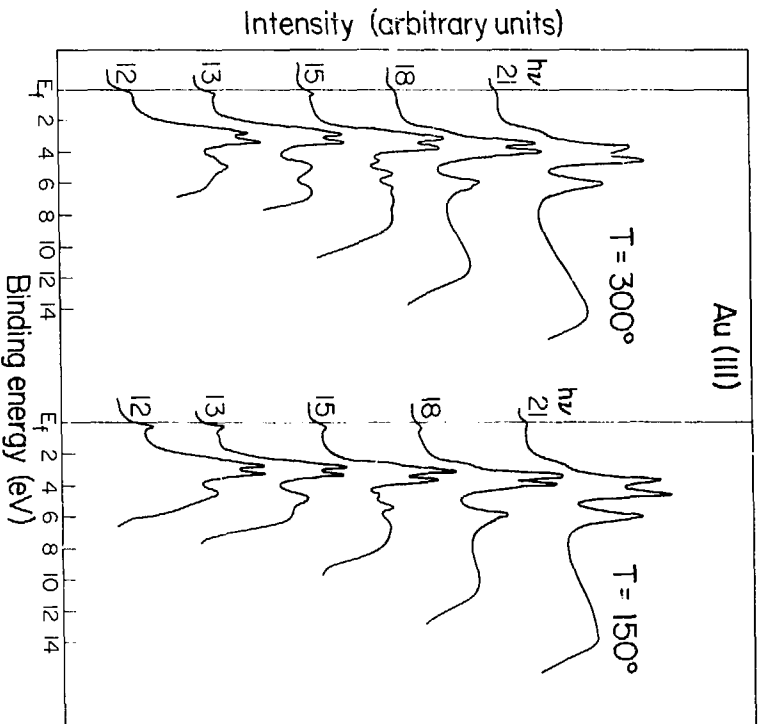


Fig. 8

XBL 797-2113

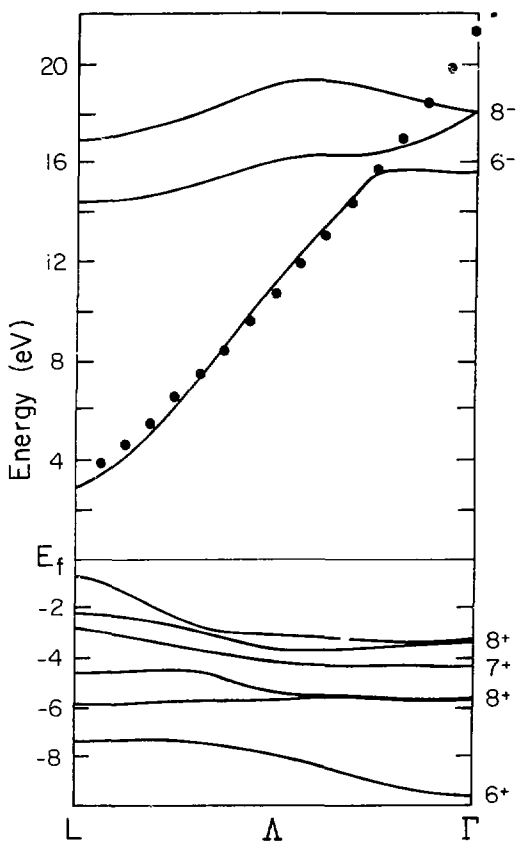
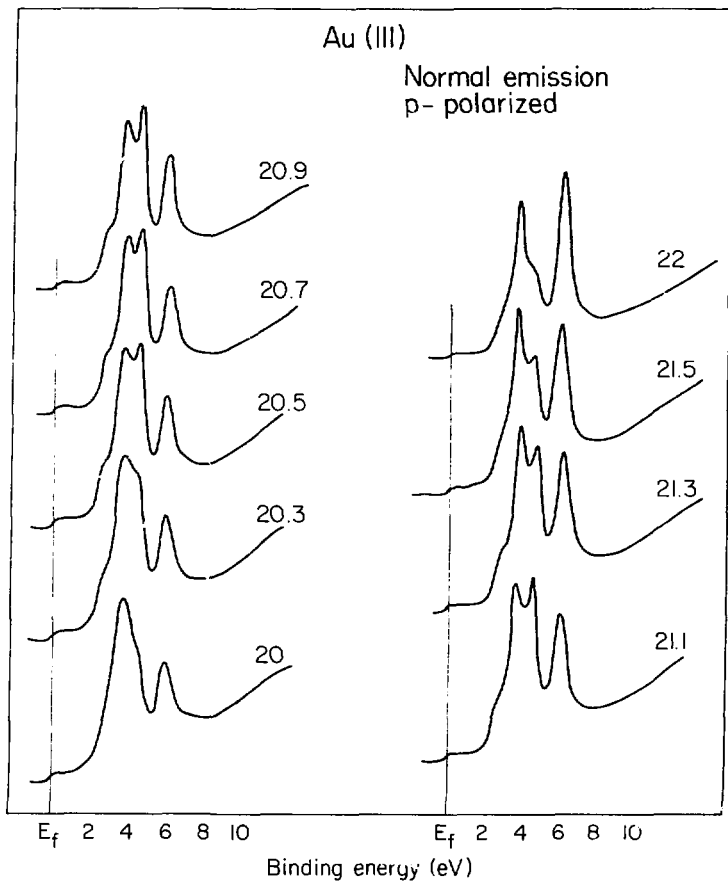


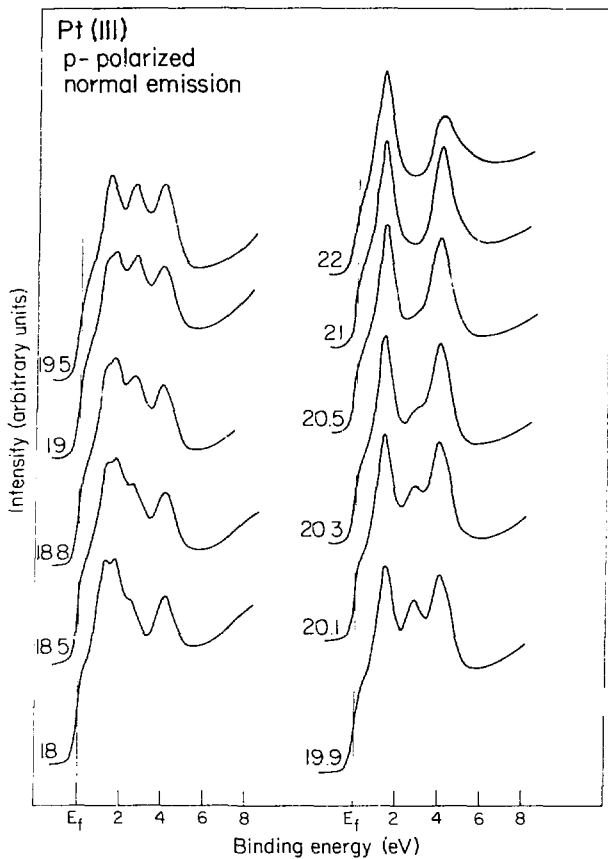
Fig. 9

XBL 797-2110



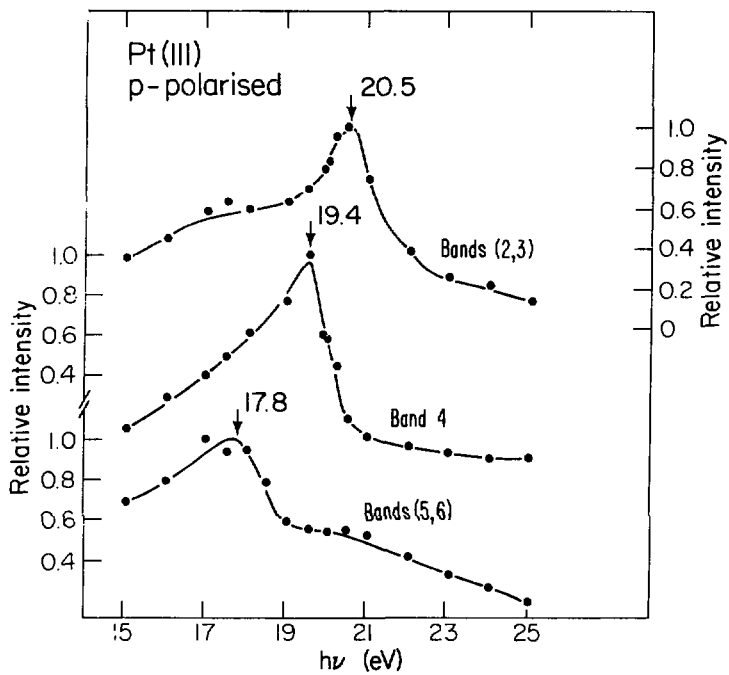
XBL 797- 2115

Fig. 10



XBL 797-216

Fig. 11



XBL 797-2105

Fig. 12

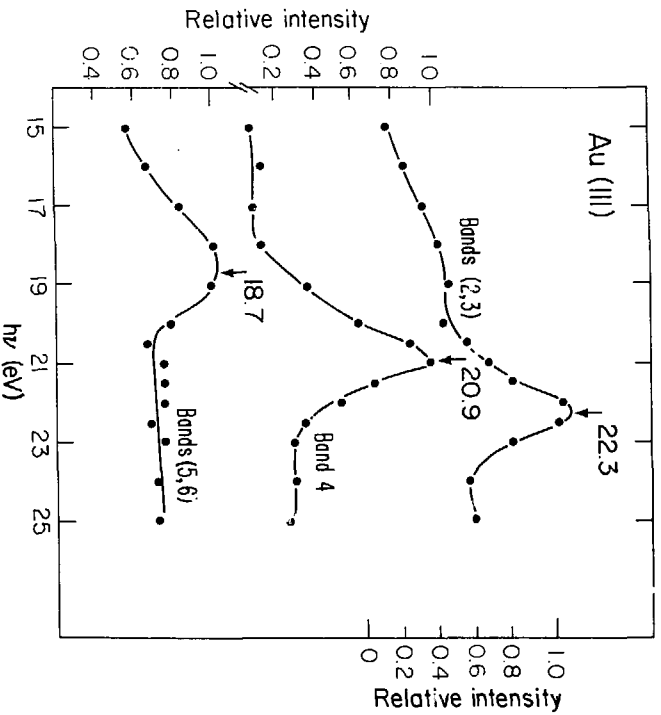
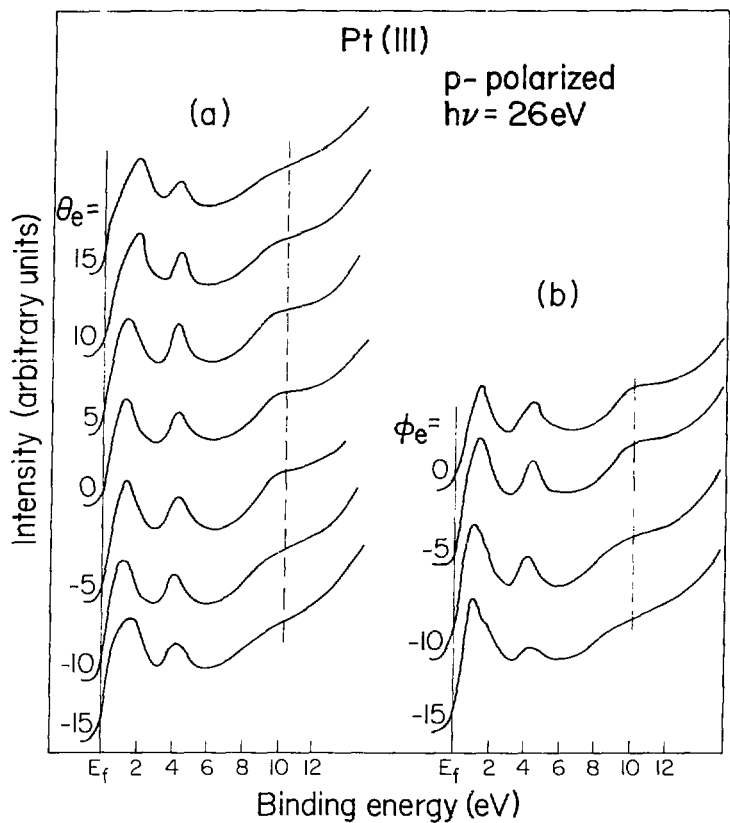


Fig. 13

XBL 797-2106



XBL 797-2114

Fig. 14

V. EMPIRICAL BANDS AND FINAL-STATE EFFECTS FOR
THE (110) AND (100) FACES OF Ag

One of the current questions in the literature of angle-resolved photoemission (ARP) is the extent to which ARP data, in conjunction with the direct transition model (DTM) and a simple quasi-free-electron final state, may be used to map dispersion relations in single crystalline metals. Studies using synchrotron radiation of the (111) face of copper,¹ nickel,² palladium,³ silver,⁴ platinum,⁵ and gold⁶ show that such an approach works well for the Γ line. Much less work has been reported, however, for the other low-Miller-index crystal faces, and there is considerable controversy concerning the details of the photoemission process for these faces. In particular, while the DTM has been used with apparent success for Cu(110)^{6,7} with photon energies up to 110 eV, it has recently been suggested that it fails for energies corresponding to excitation into conduction-band gaps.⁸

We have accordingly performed detailed studies on the (110) and (100) faces of silver, using synchrotron radiation in the photon energy range $6 \leq h\nu \leq 34$ eV. Work using laboratory sources indicates that, for the energies employed, direct transitions dominate the spectra.⁹ By using synchrotron radiation, we have been able to confirm this behavior over the entire energy range and in particular to study the gap photoemission process. As will be discussed in detail,

consideration of the binding energies and intensities of the spectral features leads to a simple physical picture which explains the observed behavior in terms of direct transitions and a quasi-free-electron final-state dispersion.

Section A gives experimental details. In Section B, the spectra are discussed, and empirical dispersion relations are presented. Section C examines the various final-state features observed, and interprets them in terms of a simple physical model for photoemission. The last section summarizes our work.

A. EXPERIMENTAL

The apparatus used has been described in detail elsewhere,^{6,10} the only change being a modification of the angular acceptance of the CMA to $\pm 2.5^\circ$. The samples were high purity silver crystals, spark-cut to produce (110) and (100) surfaces, polished to 1-micron roughness, and etched. Orientation to $\pm 1^\circ$ was achieved using back-reflection Laue photography. Final cleaning was performed in situ (base pressure in the 10^{-10} torr range) by Ar^+ sputtering and annealing at 600°K . Impurities were monitored by Auger electron spectroscopy, with an estimated detection limit of 0.05 monolayer; cleaning was continued until all major impurities (i.e., C, S, O) were near this limit.

Spectra were taken on the 8° branch line at the Stanford Synchrotron Radiation Laboratory for the geometry

shown in Figures 1 and 4, corresponding to normal emission and "p-polarized" radiation, with the electric vector in the horizontal plane defined by the Poynting vector of the light and the electron propagation direction. The angle between the latter two was fixed at 63° . The combined energy resolution (monochromator plus analyzer) varied from ca. 0.1 eV at low photon energies to ca. 0.2 eV at high energies. Count rates were typically of the order of 10^3 to 10^4 sec^{-1} , allowing most spectra to be obtained in 5 to 10 minutes.

B. SPECTRAL FEATURES AND DISPERSION RELATIONS

a. Ag(100)

Spectra for this crystal over the energy range employed are shown in Figure 1.

Perhaps the most dramatic feature observed is the set of peaks occurring for $11 \leq h\nu \leq 16$ at ca. 1-2 eV below the Fermi level (E_F). Three final states are available for transitions along the Λ line (Figure 2), corresponding to plane-wave characters of $\vec{G} = (\overline{1600})$, $(\overline{888})$ and $(\overline{888})$ for bands 7, 8, and 9, respectively (we use the units of Ref. 11, in which (800) is the X point). These latter two bands have projections of their group velocity midway along Λ of 69% and 42% along $[16,0,0]$ in free-electron approximation, and may accordingly be expected to give rise to secondary Mahan emission.^{12a} This has been observed for band 8 at $h\nu = 11$ and 11.5 using laboratory sources.⁹ The band 9 transition

onsets at $h\nu = 13.5$, confirming our expectations, and giving the assignment of $\Delta(6) \rightarrow \Delta(7)$, $\Delta(6) \rightarrow \Delta(8)$, and $\Delta(6) \rightarrow \Delta(9)$ for the overall structure. From these peaks we may estimate the spacing of bands 8 and 9, which is found to vary from 0.3 eV ($k_x \sim 5.5$) to 0.5 eV ($k_x \sim 4.8$). Secondary Mahan emission may also be expected for the more tightly bound d-bands, but will only give rise to a broadening of the primary features, since the d-bands show little dispersion for the region along Δ corresponding to these photon energies. The spectra at $h\nu \approx 11$ and 12 eV show this behavior, and in fact the d-bands could not be assigned at these photon energies.

The peak at a binding energy (E_B) of 5.6 eV, which is seen to undergo a dramatic intensity resonance at $h\nu \sim 22$ eV, is assigned to be a one-dimensional density of states (ODDOS) feature arising from band 4 (Γ_7) at Γ . The cause of this resonance will be discussed in Section IV. The other two ODDOS features expected (Γ_8 : 4.8, 5.9 eV) are not explicitly observed because they are hidden under direct transition peaks for the photon energies at which they are expected to undergo resonance. Some indirect evidence for such a ODDOS contribution exists, however, in the spectra for $h\nu \sim 23$ -26 eV; at 24 and 25 eV a marked broadening in the 6.0 eV peak is observed, which could be the ODDOS contribution at resonance of the $\Gamma_8 = 5.9$ eV level.

An interesting feature due to indirect transitions is the dispersionless peak at $E_B \approx 6.5$ eV, $15 \leq h\nu \leq 20$ eV.

The only possible origin for this is the maximum in the experimental band 1 dispersion midway along Δ (Figure 3). The intensity behavior of this peak is particularly noteworthy when compared to the direct-transition from band 1 at higher binding energy. The peak is seen to grow in relative intensity over the entire photon energy range, eventually merging with the final-state-induced direct transition resonance for band 1 at $h\nu = 23$ eV; this latter resonance, which has a characteristic half-width of ca. 1 eV,⁵ cannot explain the intensity variation. Its cause lies in the fact that, for indirect transitions, the intensity will be related to the amplitude of the phonon assisting the transition; since this amplitude increases as the phonon wavevector decreases, nearly vertical indirect transitions should be favored.^{12b} This is exactly the behavior observed.

There are some isolated features at low photon energies that cannot at present be explained. In particular, for $h\nu = 11$ eV, weak and broad features at 1.4 and 2.7 eV binding energy are observed. Their recurrence at 12 eV cannot be ascertained, as they would be hidden by the contribution of second-order light to the background, which cannot be removed for $h\nu > 11.6$ eV. At $h\nu = 13$ eV, a weak shoulder is observed for $E_B = 3.3$, and at $h\nu = 14$ and 15 eV, a weak peak for 2.9 eV binding energy. All these features are minor, corresponding to less than 100 counts over background. They could arise from several sources, including those

related to the energy analyzer, random fluctuations in the synchrotron radiation flux, or actual physical processes such as some sort of loss mechanism for the band 6 resonance.

The remaining spectral features are all due to primary-cone direct transitions. The band 6 peak is seen to disperse rapidly with photon energy, merging with the d-bands by ca. 21 eV photon energy. Intensity resonances are visible in the photon energy range $22 \leq h\nu \leq 24$ eV, as expected from studies of the (111) face of Pt, Au, and Ag,^{4,5} yielding $\Gamma_{6-}(7) = 16.8$ eV, in excellent agreement with theory. We have assigned the DTM features in an analogous manner to that previously described.⁵ The choice of final state was once again a quasi-free-electron fitted to the RAPW calculation (Figure 2), with $m^* = 1.10 m_e$ and $V_0 = -2.4$ eV. All primary emission occurred for initial states in the second Brillouin zone; $\vec{G} = (\overline{1}600)$ connected the initial and final states via $\vec{k}_f = \vec{k}_i + \vec{G}$. The Fermi level was determined as before,⁵ by a combination of spectral assignment and comparison of reference voltages; the RMS scatter of the derived work function was ± 0.05 eV. Our spectra agree well with those of Hansson and Flodstrom,⁹ except that, once again, there is a 0.2 eV discrepancy in the binding energy, most likely due to a difference in angular resolution and in the assignment of E_F .

Figure 3 and Table I give the empirical dispersion relations obtained. Agreement with the theoretical RAPW

calculations¹¹ is generally good; the major discrepancy is in the s-p band, which is seen to disperse somewhat more sharply than expected. The assignment of the transition $\Delta(2) + \Delta(7)$ for $h\nu < 20$ eV is complicated by the indirect-transition peak at 6.5 eV discussed earlier; the repulsion of bands (1,2) midway along Δ is larger than theoretically predicted, but difficult to quantify. The band 6 mapping could be brought into better agreement with theory by altering the final-state parameters; such a procedure would be ad hoc, however, and it is more instructive to use the fit as given above. For Ag(110), to be discussed below, our spectra extend through the X point along Σ' , which enables a modification of the final state based on general symmetry arguments. This analysis will indicate that our choice of an unmodified fit to the RAPW band is probably not the best one possible.

The selection rules for these spectra are easily derived by arguments analogous to those for Pt(111)⁵; all initial states are sampled for s-polarized radiation ($\xi \parallel [100]$), and only Δ_5 for pure p-polarization ($\xi \perp [100]$). Accordingly, for the mixed polarization present in these studies, all states should be observable. The disappearance of band 4 for $k_x \leq 4$ is thus probably due to a masking of the $\Delta(4)$ peak in the energy range $22 \leq h\nu \leq 25$ by the stronger $\Delta(5)$ direct transition resonance, and by a resonance in the ODDOS peak attributable to Γ_7 . Band 3 is also not observed, presumably for cross-section reasons.

b. Ag(110)

Spectra are shown in Figure 4 for this face, $6 \leq h\nu \leq 34$.

A surface state at $E_B = 0.2$ eV is clearly visible in the spectra for $h\nu = 6-9$ eV; it has not been reported in the previous work of Hansson and Flodstrom.⁹ This peak was reproduced, along with all other spectral features, in two independent experiments, and its angular dependence was investigated. The intensity of this feature was maximal for normal emission, being attenuated by 60% for emission at a polar angle of 10° off normal. While we did not perform the adsorbed gas test sometimes used to characterize surface states,¹³ spectra obtained during the cleaning process (which required three cycles of bombardment and annealing) clearly showed that the presence of even trace amounts of sulfur on the surface led to a factor of 3 loss in intensity for this peak. Presumably, this feature was missed in the work of Ref. 9 due to inadequate sample preparation. In that study, the only criterion of sample cleanliness was constancy of the spectral appearance before and after cleaning, which is a less reliable criterion than the use of AES, since the trace contaminants that can alter surface properties will not necessarily affect bulk features.

Secondary Mahan emission contributes significantly to these spectra, and is in fact virtually the only direct transition photoemission allowed at these energies along

the Γ (Γ -K) line; primary cone emission is restricted to Γ (K-X). Figure 5 shows the RAPW band structure.¹¹ Along Γ , the plane-wave character of bands 7, 8, and 9 is $\vec{G} = (8,8,8)$, $(8,8,\bar{8})$, and $(16,0,0)$, respectively. Primary emission, corresponding to a band with $\vec{G} = (16,16,0)$, will only onset from band 6 for $h\nu \approx 30$ eV. The plane-wave-derived group velocities of bands 7, 8, 9 midway along Γ , have projections along $(16,16,0)$ of roughly 40%, 40%, and 30%, respectively. While band 9 might thus be presumed to contribute some emission, it is in fact not observed to do so; bands 7 and 8 account for all the secondary-cone features observed. Two features associated with secondary emission are particularly noteworthy. First, the s-p transitions $\Gamma(6) \rightarrow \Gamma(7)$ and $\Gamma(6) \rightarrow \Gamma(8)$ are observed for $7 \leq h\nu \leq 10$, as weak but clearly discernible peaks. Second, analogous to the behavior of primary cones for the (111) and (100) faces, the secondary cones are also seen to undergo intensity resonances near Γ , as evident in the spectra for $h\nu = 20 - 24$ eV. In fact, the spectra in this range contain a total of 8 peaks at each energy due to primary and secondary cone direct transitions, which is representative of the richness of features observed for this face. It is interesting that the s-p resonance was not observed for the study reported in Ref. 1; this may be a result of modification of the surface unklapp process required for secondary-cone emission because of surface contamination.

The structure near E_F for $h\nu \geq 30$ eV may be due to several sources. In order to more fully investigate it, spectra were taken at normal and nonnormal emission, as shown in Figure 6. Unfortunately, this feature only begins to develop at the upper energy limit of the 8° line monochromator, where both count rate and resolution are poor; this made it impossible to follow its evolution sufficiently to provide a definitive assignment. It is likely, however, that one of the constituent peaks is the band 6 resonance for primary emission. This feature is expected to be weak at these photon energies, since the d character of band 6 near E_F along Σ (as determined by an LCAO interpolation-scheme calculation¹⁴) is roughly an order of magnitude less than for copper, in which the band 6 resonance is of roughly equal intensity in comparison to the d-bands.¹⁵ Unlike in Cu, the band 6 d-character in Ag does not change significantly as \vec{k} varies away from Σ , so that off-normal emission cannot be used to identify the s-p peak.

Another constituent of this structure may arise from surface-state photoemission. As is seen, the leading peak of this feature is dispersionless, falling at $E_B \sim 0.4$ eV. In a simple model of ARP for surface states,¹⁶ the initial state may be considered as an exponentially damped periodic function. Evaluation of the transition matrix element for a plane-wave final state then amounts to the evaluation of the Fourier transform of the initial state. This results

in the prediction of a rapid intensity modulation of the surface-state peak, as is commonly observed at low ($h\nu \leq 11$ eV) photon energies. Higher harmonics in the fourier transform, however, would allow the feature to reoccur; heuristically, we might expect the second harmonic at roughly four times the photon energy, or in this case at roughly 30-40 eV. Results on Cu(111) have shown the existence of a surface state near E_F at photon energies of ca. 70 eV photon energy, which could be due to such a recurrence.¹⁷ That the Ag(110) peak at 0.3 eV, $h\nu \geq 30$ eV, diminishes off normal, is consistent; however, it does not appear to be particularly sensitive to surface contamination, having nearly equal intensity throughout the cleaning process. In addition, from the spectra at 33 and 34 eV, it is clear that more than two peaks are present in this structure; the band 6 resonance and photoemission from only one surface state, then, cannot be sufficient for a complete explanation. A definitive study must await a monochromator with adequate flux and resolution in the range $30 \leq h\nu \leq 50$ eV.

Figure 7 and Table II give the empirical dispersion relations derived from these data. The procedure was identical to that used for the (100) data, with the exception of the choice of final state. Since the primary-emission (110,16,0) conduction band was not calculated in the RAPW band structure,¹¹ we fitted band 7, obtaining $m^* = 1.05 m_e$ and $V_0 = -3.5$ eV. Using these values to calculate the

primary emission final state did not give symmetrical initial state dispersion relations about X, and placed the s-p band far away from the RAPW prediction. We thus altered m^* and V_0 to obtain this symmetry and optimize the comparison with the theoretical valence bands yielding $m^* = 0.95 m_e$ and $V_0 = -7.3$ eV. As shown in Figure 5, this choice gives a band which midway along Σ is quite similar to the RAPW one, but shifted down by roughly 2 eV; we will discuss a possible explanation in Section C. With this choice of final state, the agreement between the RAPW and empirical valence-band dispersion relations is quite good, with the largest deviation (ca. 0.25 eV) being once again in bands 1 and 2. We note that the mapping along Σ is subject to greater uncertainties than that along Σ' , since it is derived almost exclusively from secondary cone emission, which in many cases gave weak peaks or shoulders that were difficult to assign in binding energy. In addition, the flatness of the bands near Γ would indicate the possibility of ODDOS features, which would further complicate the analysis. Peaks which could be due to either a ODDOS or direct-transition mechanism are so indicated in Figure 5.

C. FINAL STATE EFFECTS

The existence of the intensity resonances reported both here and elsewhere for Ag, Au, and Pt^{4,5} indicates that these features may be expected to occur whenever the bulk conduction

bands become flat, which most typically occurs near the edge of a gap at a symmetry point. While it is tempting to assign the resonances to a high final density of states (DOS), such an interpretation is clearly inconsistent with our use of a quasi-plane-wave dispersion relation, for which the DOS varies smoothly as $E^{1/2}$. It is necessary, then, to consider this process in detail, and the related processes of ODDOS and band-gap photoemission, in order to obtain a consistent explanation.

To proceed with this discussion, we consider a simple physical picture which specifically invokes the surface-sensitive nature of photoemission in this energy domain. The final state in the crystal must couple with a plane wave in the vacuum, and in fact this coupling is requisite for band-gap photoemission, which would be rigorously forbidden in the infinite-solid limit. We assume that, close to the surface, the dispersion relation of a conduction electron with parallel that of the free electron in vacuum, the only difference being a shift in energy, taken to be constant, to account for the effect of the bulk and surface potentials. We further assume that the valence-band dispersion is unaffected by the surface. This is equivalent to approximating the surface potential as a step function; there will then be no itinerant bound states in the vacuum, and the effect of the surface on a valence-band wavefunction will be to change its phase, but not its wavevector.¹⁸

As is well-known, a plane wave in vacuum may be expanded in terms of spherical harmonics and Riccati functions. Given our assumption of final-state plane-wave-like behavior in the crystal, we may expand the final state analogously

$$|E_f, \vec{k}_f\rangle \sim \sum_{\ell, m} a_{\ell m}(r) Y_{\ell m}(\vec{k}_f) Y_{\ell m}(\vec{r}) \quad (1)$$

where the $a_{\ell m}(r)$ are now unknown functions determined by the crystal potential. We suggest that the effect of the crystal potential near the surface will be to alter the angular momentum composition, but not the dispersion, of the final state. In the theoretical bands, the flattening observed at Γ_6^- is due to mixing of f-like components,²⁰ which would then correspond to an increase of a_{3m} in the expansion above.

It follows immediately that the intensity resonances are a consequence of the photoemission cross-section, and not the final density of states. The initial state will be primarily d in character; the cross-section is then

$$\sigma \sim \sum_{m=-\ell}^{\ell} \langle E_f, \vec{k}_f | \vec{A} \cdot \vec{\nabla} | n, \ell = 2, m \rangle$$

and in dipole approximation, the Wigner-Eckhart theorem implies that only $\ell=1$ and $\ell=3$ components in the final state will contribute.²¹ Accordingly, mixing near Γ of $\ell=3$ components into the final state should cause the cross-

section to undergo resonance, as is observed. It is important to note that this alteration of the angular momentum composition of the final state is not inconsistent with constancy of its dispersion; the "s-p" band 6, for example, continues to disperse much as a plane wave even though its d character changes dramatically. In silver, for example, band 6 along Σ fits a quasi-plane-wave equation with $m^* = 0.97 m_e$, $V_0 = -5.6$ eV, while along Δ we have $m^* = 0.87 m_e$, $V_0 = -6.4$ eV; however, this band has three times as much d-character along Σ as it does along Δ , even though m^* is closer to m_e along Σ .

There are several consequences of such a model. The first concerns features due to an ODDOS mechanism; while k-conservation is no longer required for such a mechanism, the cross-section argument given above will still be applicable. Accordingly, features which are nominally assigned to an ODDOS process will still be expected to undergo intensity resonances at those photon energies corresponding to nearly vertical transitions into a final state of higher ℓ character. This is not just formally equivalent to an enhanced contribution from direct transitions; while an experimental verification would be extremely difficult, it is conceivable that, for a very steeply dispersing initial-state band, one could separate these effects, with the direct transition contribution dispersing over the resonance, and the ODDOS contribution falling at constant energy. In the

case of our spectra for Ag(100), resonances in a peak assigned to an ODDOS process ($E_p = 5.6$ eV) are observed, but no such deconvolution is possible.

The second consequence of our model is to remove the ad hoc nature of the shift in V_o employed for the (110) face. The bulk contribution to the shift in energy assumed above is accounted for by fitting the RAPW bands, but the surface term is not. This last term, expected to be roughly comparable to the work function, must also be subtracted to yield the final-state dispersion, and this subtraction is accounted for by the 3.8 eV difference between the fitted value of V_o and the final value employed. This is of course a very simplistic picture, both since the value of V_o is coupled to m^* , and because the details of the surface perturbation are far more complicated than a mere work-function correction would predict. The qualitative content seems valid, however, and would indicate that such a shift will be expected for all crystal faces, although its magnitude will depend on the face under study.

The most interesting consequence of our model is that it predicts a continuation of direct transitions, as mirrored by dispersion of spectral features, for photon energies corresponding to bulk band-gap photoemission. This is in contradiction to the analysis of Dietz and Himpsel for Cu(110).⁸ We believe this contradiction is directly related to the choice of final state. Dietz and Himpsel used the

theoretical bulk conduction bands exactly as calculated; if we include a shift of roughly 5 eV (the value used in Ag(110), scaled for the difference in lattice constants) in the fitted value of V_0 for Cu(110), the center of the dispersionless region for bands 3 and 4 falls at the X point. With this choice of final state, then, the lack of dispersion in Cu(110) is simply a reflection of the flatness of bands 3 and 4 near X. In fact, since the d bands are not as flat near X in Ag(110), this crystal provides a better test of spectral dispersion for "band-gap" photoemission; as is seen in Figure 7, bands 3 and 5 clearly disperse for gap photoemission ($11 \leq h\nu \leq 16$), as do bands 1 and 2 ($13 \leq h\nu \leq 18$). Further, for the (100) crystal, bands 1 and 2 are also seen to disperse ($23 \leq h\nu \leq 28$) in the gap expected at Γ . It is important to note that, given the shape of the d bands along Σ' , a different choice of final state will not alter this conclusion; essentially, there is nowhere along this line where the range of initial-state vectors corresponding to a gap of ca. 5 eV will allow dispersionless direct transitions, as is the case in Cu. Thus, photoemission at energies corresponding to bulk final-state gaps is still dominated by direct transitions; it seems plausible to suggest that this is a direct consequence of the close proximity of the vacuum, and the attendant coupling of the final state inside the surface with that outside.

D. SUMMARY

We have presented results of variable photon energy ARP studies of Ag(110) and Ag(100). Empirical dispersion relations, in generally good agreement with the results of RAPW calculations, have been derived, based on both primary and secondary cone emission features. Consideration of the final-state features has led to a simple physical picture that validates the use of a quasi-free-electron final state. This picture accounts for the existence of intensity resonances associated with bulk final-state features, makes plausible the discrepancy between the theoretical RAPW conduction bands and those used empirically, and explains the existence of initial-state dispersion for bulk band-gap photoemission. In combination with prior work for the (111) face, these results enable us to present an empirical valence-band structure for silver along all the principal symmetry lines.

REFERENCES

- 1) D.A. Shirley, R.S. Williams, P.S. Wehner, R.F. Davis, and S.D. Kevan, Phys. Lett. A, to be submitted.
- 2) F.J. Himpsel, J.A. Knapp, and D.E. Eastman, Phys. Rev. B19, 2919 (1979).
- 3) F.J. Himpsel and D.E. Eastman, Phys. Rev. B18, 5236 (1970).
- 4) P.S. Wehner, R.S. Williams, S.D. Kevan, D. Denley, and D.A. Shirley, Phys. Rev. B19, xxxx.
- 5) K.A. Mills, R.F. Davis, S.D. Kevan, G. Thornton, and D.A. Shirley, Phys. Rev. B, to be submitted.
- 6) J. Stöhr, P.S. Wehner, R.S. Williams, G. Apai, and D.A. Shirley, Phys. Rev. B17, 587 (1978).
- 7) P. Thiry, D. Chandesris, J. LeCante, C. Guillot, E. Pinchaux, and Y. Petroff, Phys. Rev. Lett. 43, 82 (1979).
- 8) E. Dietz and F.J. Himpsel, Solid State Comm. 30, 235 (1979).
- 9) G.V. Hansson and S.A. Flodstrom, Phys. Rev. B17, 473 (1978).
- 10) P.S. Wehner, PhD Thesis, Univ. of California, Berkeley, April 1978 (LBL-7622).
- 11) N.E. Christensen, Phys. Stat. Solid B54, 551 (1972).
- 12) a) G. Mahan, Phys. Rev. B2, 2452 (1971).
b) F.J. Shevchik, Phys. Rev. B16, 3428 (1977).

- 13) B.J. Wacławski and E.W. Plummer, *Phys. Rev. Lett.* 29, 783 (1972).
- 14) L. Hodges, H. Ehrenreich, and N.D. Lang, *Phys. Rev.* 152, 505 (1966), using the parametrization of N.V. Smith, *Phys. Rev.* B3, 1882 (1971).
- 15) J. Stöhr, P.S. Wehner, R.S. Williams, G. Apai, and D.A. Shirley, *Phys. Rev.* B17, 587 (1978).
- 16) R.S. Williams, PhD Thesis, Univ. of California, Berkeley, May 1978 (LBL-7676).
- 17) Y. Petroff, private communication.
- 18) See, e.g., A. Messiah, *Quantum Mechanics* (Amsterdam, North Holland, 1958), Chapter III.
- 19) A. Messiah, *op. cit.*, Chapter IX.
- 20) J. Hermanson, J. Anderson, and G. Lapeyre, *Phys. Rev.* B12, 5410 (1975).
- 21) M. Tinkham, *Group Theory and Quantum Mechanics* (New York, McGraw-Hill, 1964), Chapter 5.

Table I
Empirical Band Energies Along Δ in Silver (eV)

k^a	Band 1	Band 2	Band 3	Band 4	Band 5	Band 6
100	-	5.90	-	-	4.90	-
300	6.58	6.05	-	-	4.82	4.45
400	6.60	6.28	-	5.00	4.48	3.50
500	6.85	6.47	-	4.60	4.25	1.80
700	6.90	6.55	-	4.30	3.87	-
E_{\min}^b	7.05	6.58	-	5.10	4.90	4.50
$(k_x)_{\min}^b$	6.10	6.30	-	3.40 ^c	2.75	2.80 ^c

^aUnits of Ref. 11

^bValues of E_B and k_x for experimentally accessible regions along Δ where band is most tightly bound.

^cNot a true minimum--see Figure 3.

Table II
 Empirical Band Energies along Σ and Σ' in
 Silver (eV)

k^a	Band 1	Band 2	Band 3	Band 4	Band 5	Band 6
000	-	6.15	6.15	5.50	-	-
220	6.65	6.00	-	5.28	4.95	-
330	6.45	-	-	-	4.95	-
440	-	6.05	5.35	5.10	4.75	1.65
666	7.00	-	5.28	4.70	4.28	-
181	7.20	6.88	4.65	4.30	4.05	-
080	7.35	7.00	4.20	-	3.90	-
E_{\min}^b	7.35	6.15	6.15	5.50	5.00	2.55
k_{\min}^b	(8,0,0)	(0,0,0)	(0,0,0)	(0,0,0)	(2.3,2.3,0)	(3.7,3.7,0)

^aUnits of Ref. 11.

^bValues of E_B and k chosen from experimentally accessible regions along Σ and Σ' where band is most tightly bound.

^cNot a true minimum--see Figure 7.

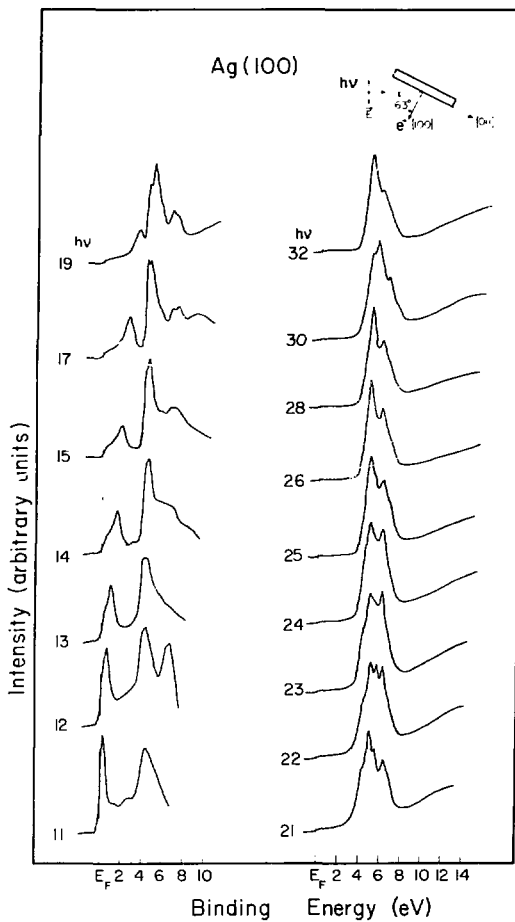
FIGURE CAPTIONS

- Fig. 1. Selected normal emission spectra for Ag(100) in the photon energy range $11 \leq h\nu \leq 32$ eV. The inset gives the experimental geometry.
- Fig. 2. Theoretical RAPW bands (solid lines, Ref. 11) and quasi-free-electron final state used (circles) for Ag(100).
- Fig. 3. Empirical dispersion relations (circles) and theoretical bands (lines) for Ag along Λ . The scale at the top gives the final state, shifted down by the indicated photon energy. The k vectors given for Γ and X indicate that all final states are in the second zone, with $k_f = k_i + (\overline{16}, 0, 0)$.
- Fig. 4. Selected spectra at normal emission for the photon energy range $6 \leq h\nu \leq 33$ eV for Ag(110). The inset gives the experimental geometry.
- Fig. 5. Band structure of Ag along Σ and Σ' . The solid lines are the RAPW result (ref. 11). Circles are the quasi-free-electron final state used for primary emission ($\vec{G} = (\overline{16}, 16, 0)$), and squares the quasi-free-electron final state used for secondary emission ($\vec{G} = (8, 8, 8)$). For the latter, two final-state bands were generated by displacing the quasi-free-electron band uniformly up or down by 0.25 eV.

Fig. 6. Spectra at normal emission and 10° off normal for Ag(110) in the energy range $30 \leq h\nu \leq 34$ eV. The structure at low binding energy is shown expanded by the indicated factor.

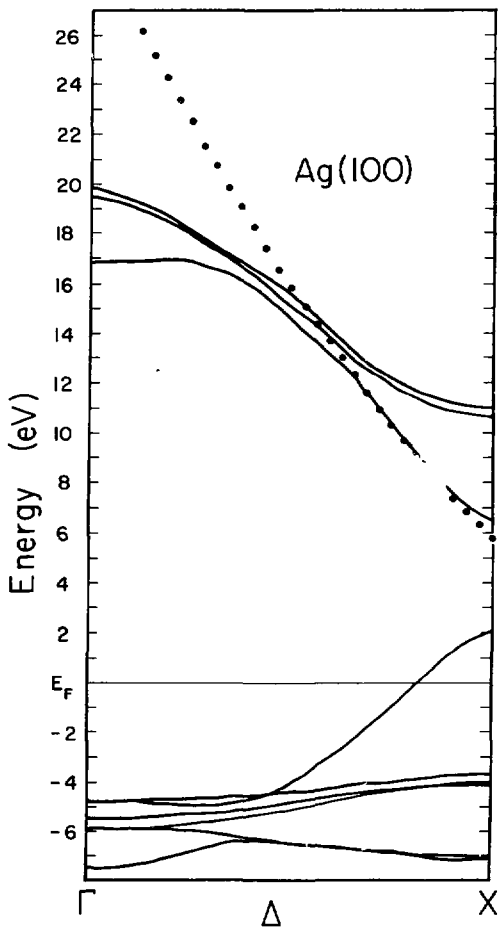
Fig. 7. Empirical dispersion relations for silver along Σ and Σ' . Filled circles are derived from primary emission, squares from secondary emission. Open circles are due either to secondary emission or an ODDOS mechanism. Solid lines are the RAPW results (Ref. 11). Primary and secondary cone final states are given by the scale at the top.

Fig. 8. Empirical band structure (circles) of silver. The RAPW bands (solid lines, Ref. 11) are shown for comparison. Data for the Λ line is from Ref. 4.



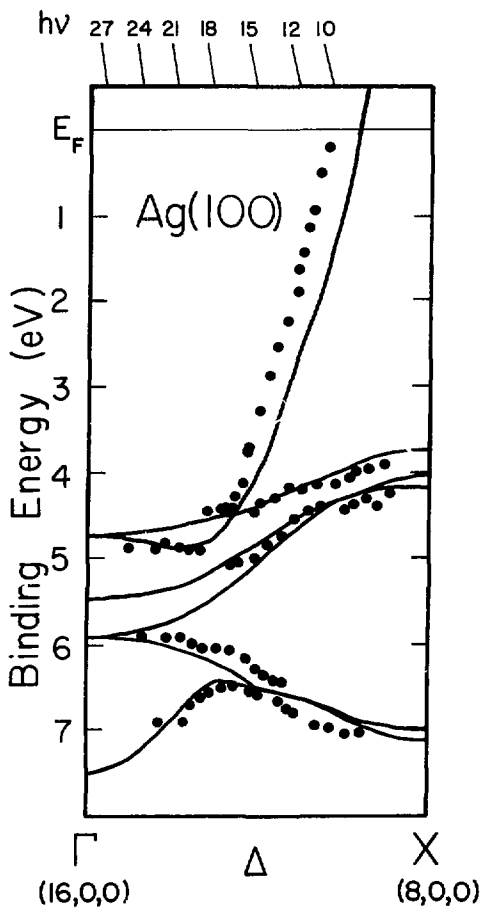
NBL 797-10716

Fig. 1



XBL 797-10719

Fig. 2



XBL 797-10722

Fig. 3

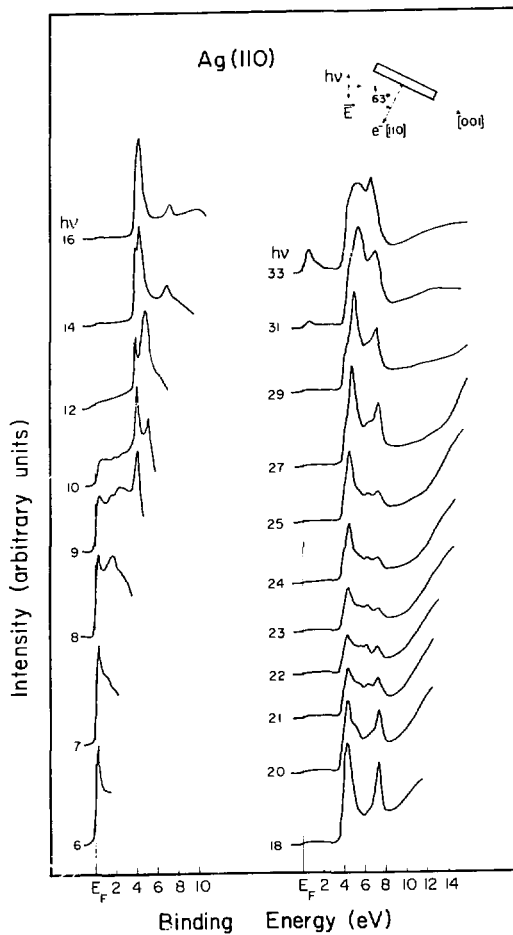
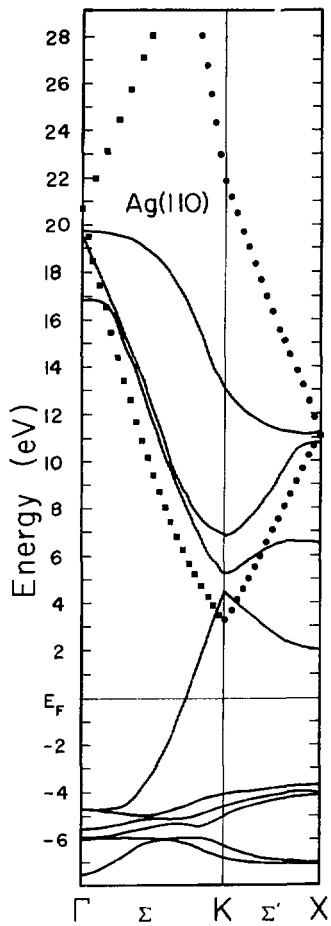


Fig. 4



XBL 79/-10720

Fig. 5

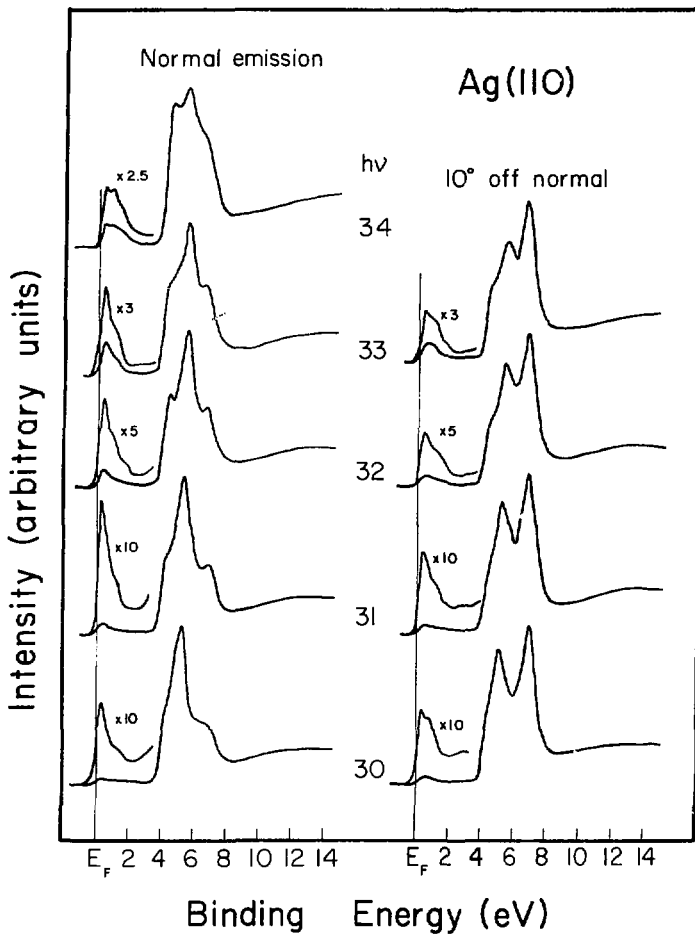


Fig. 6

XBL 797-10718

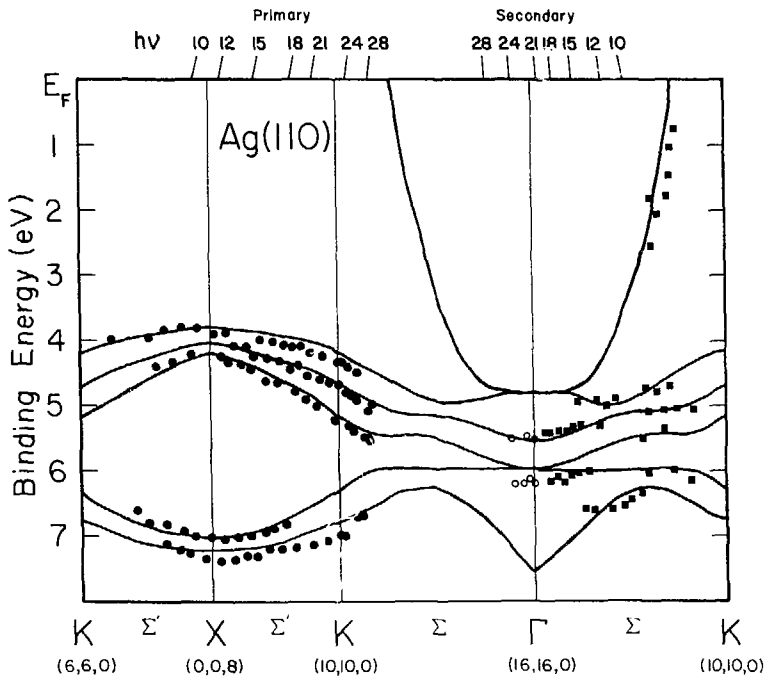


Fig. 7

LBL 797-10721

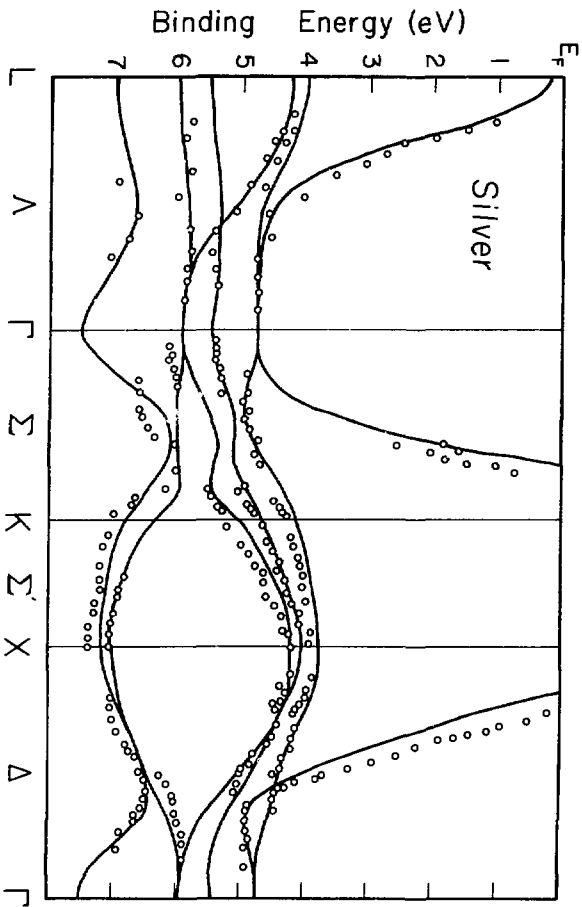


Fig. 8

XBL 797-10723

Our praises are our wages.

A Winter's Tale, i, 2.

ACKNOWLEDGMENTS

While a work of art may derive from the creativity of a single mind, such is rarely the case for a doctoral thesis in the physical sciences. The acknowledgment of this interplay should be neither a *pro forma* exercise in self-effacement, nor a sycophantic artifice for engendering approbation, but simply recognition of the diversity of individual talents, and the importance of their commingling for both one's personal and professional growth.

The importance of the thesis advisor is almost axiomatic. I have been fortunate to work with Professor David A. Shirley, not because these labors have always been facile or pleasant, for they have not, but because of the freedom and opportunity which he provides to pursue one's own ideas and goals. I value the independence and critical facility which this engenders.

A collaborative effort is only as successful as the quality of its participants. It is accordingly with pleasure that I acknowledge Mr. David R. Denley and Mr. Richard F. Davis, my most intimate colleagues for the past eighteen months. We have not always agreed on matters of procedure or

interpretation, but I have never had cause to doubt their professional excellence. I have also profited from interaction with Drs. Paul S. Wehner, Geoffrey Thornton, Paolo Perfetti, and Rand Watson, and Mr. Steven D. Kevan. The support staff of both the Lawrence Berkeley Laboratory and the Stanford Synchrotron Radiation Laboratory have been of real value in assisting the progress of this work; if they have only 'done their job', it is gratifying nonetheless to acknowledge a job competently done in an era of ascendent mediocrity. Two members of the LBL staff, in particular, must be mentioned: Mrs. Winifred Heppler and Mrs. Karen Janes, who have not only performed their duties with skill, but have made the Laboratory a more congenial working place into the bargain.

For their friendship, intellectual stimulation, and impact on my most fundamental tenets, my gratitude: Rita and Maury Mills, Pat and Leslie Perkins, and John and Paula Swanson.

It is well to remember that the completion of a doctorate represents not a culmination of scholarship, but only its commencement. Departure from the academic milieu should not imply repudiation of its precepts; to do so is to risk vitiating what was at such toil obtained. "A little learning

is a dangerous thing ", wrote Pope in his *Essay on Criticism*,

*Drink deep, or taste not the Pierian spring;
There shallow draughts intoxicate the brain;
And drinking largely sobers us again.
Fired at first sight with what the Muse imparts,
In fearless youth we tempt the heights of Arts,
While from a bounded level of our mind
Short views we take, nor see the lengths behind;
But more advanced, behold with strange surprise
New distant scenes of endless science arise!*